University of Nevada, Reno

Effects of surface mass loading on the stochastic properties of GPS time series in the Great Lakes region

A thesis submitted in partial fulfillment of the
requirements for the degree of Master of Science in
Geophysics

by

Jordan A. Krcmaric

Dr. Corné Kreemer
Thesis Advisor

May, 2024

THE GRADUATE SCHOOL

We recommend that the thesis
prepared under our supervision by

entitled

be accepted in partial fulfillment of the
requirements for the degree of

Advisor

Committee Member

Graduate School Representative

Markus Kemmelmeier, Ph.D., Dean
Graduate School

Abstract

Daily Global Positioning System (GPS) time series provide a critical dataset for studying the Earth. In the past decade, an explosion in the number of continuously operating GPS stations combined with improved processing strategies have enabled the detection of ground motions with rates of less than 1 mm/yr. However, detecting such subtle rates in GPS time series is complicated by the presence of errors and other effects that introduce stochastic variability and increase rate uncertainty. Some of this stochastic variability is due to surface mass loading, which causes displacements in GPS time series from atmospheric pressure fluctuations, oceanic mass redistribution, and changes in hydrology. This thesis investigates the effect of surface mass loading on 2,481 GPS station time series around the Great Lakes region of the U.S. and Canada. This region is ideal for studying the effects of surface mass loading because it is covered by a dense network of GPS stations that capture ground displacements due to fluctuations in water levels within the Great Lakes. Uncorrected GPS time series are compared to time series that have been corrected with models of surface mass loading using 4 metrics: variance reduction in corrected residual time series; white, flicker, and random walk noise amplitudes; station velocity uncertainties; and average power spectra of residual time series. Common mode component (CMC) filtering is a method used to remove spatially correlated signals from GPS time series. I also compare CMC filtered time series to see if filtering methods are effective at removing surface mass loading. Finally, to understand the role that GPS station monument type plays in the stochastic variability of the time series, I compare noise amplitudes and velocity uncertainties of 5 categories of monuments: deep-drilled braced monuments, roof mounted, concrete pillars, steel towers, and any monument directly anchored in bedrock. Results show that non-tidal atmospheric and ocean loading (NTAOL) is responsible for the most significant proportion of variance in GPS time series, and correcting for NTAOL reduces the median flicker noise amplitudes by ~50%. However, median white and random walk noise amplitudes increase in NTAOL corrected time

series due to a masking effect by NTAOL in the uncorrected time series. Correcting for hydrological loading reduces both variance and random walk noise amplitudes most significantly in GPS stations closest to the Great Lakes. Correcting for both NTAOL and hydrological loading decreased the median velocity uncertainty from 0.35 mm/yr to 0.18 mm/yr. There are no significant differences in variance reduction or stochastic properties between CMC filtered time series whether they have been corrected for surface mass loading or not, indicating that most of the variability due to surface mass loading is removed in the filtering process. When compared to time series that are not filtered, CMC filtering reduces both median white and flicker noise amplitudes, but median velocity uncertainty changes very little due to an increase in random walk noise amplitudes in some filtered time series. A comparison of monument types using the CMC filtered time series shows that out of the two most common monument types in the study region, roof mounted and concrete pillars, roof mounted monuments have a lower median velocity uncertainty. However, concrete pillar monuments in Michigan outperform other concrete pillar monuments and most roof mounted monuments, indicating that the design of concrete pillar monuments plays a crucial role in the stability of the station. A seasonal signal correlated to temperature was found to be present in some stations, particularly in the states of Wisconsin and Minnesota. The implications for this temperature seasonal signal and a potential method for correcting it, in order to extract only the hydrological related seasonal signal from GPS time series, is discussed.

Acknowledgements

There are several people I would like to thank for supporting me during my master's degree work at UNR. First, I would like to thank my advisor, Dr. Corné Kreemer, for his excellent guidance. He allowed me the freedom to pursue my interests while always providing input that led me in the right direction. Next, I would like to thank my committee members Dr. Geoff Blewitt and Dr. Anna Panorska for agreeing to serve on my thesis committee and providing suggestions that improved the quality of my thesis. Dr. Bill Hammond also deserves thanks for the instruction he provided me at UNR and for discussions that also contributed to the work presented in this thesis.

I would not be attending graduate school at UNR without the support of the U.S. National Geodetic Survey and their advanced degree program for employees. I specifically want to thank all the people that served as my supervisor during the program; Dr. Jacob Heck, Dr. Xiaopeng Li, Dr. Andria Bilich, and Dr. Shachak Pe'eri. Their support was one of the reasons for my success in my graduate studies.

Finally, I would like to thank my family and friends, the only reason I have made it this far is due to their constant support and love. Most of all my partner Melissa Schwan, who is always there for me and always believes in me, even when I don't believe in myself. I could not have done this without her.

Table of Contents

List of Tables

List of Figures

Chapter 1: Introduction

1.1 Motivation and objective

For over 3 decades now, Global Positioning System (GPS) observations have been used to study and model the movement of the Earth's crust. The number of GPS stations around the world has exploded in recent years (Blewitt et al., 2018), and combined with improved processing strategies this has enabled the detection of subtle ground motions with rates below 1 mm/yr (Masson et al., 2019). The ability of GPS to detect these subtle motions has led to significant contributions in a variety of scientific fields (Bock and Melgar, 2016), most notably in the fields of geodynamics and tectonics where small changes in horizontal and vertical motions has revealed new insights into processes in the deep interior of the Earth (Kreemer et al., 2020). However, extracting these subtle motions is complicated by the presence of errors and other signals that introduce stochastic variation into the GPS time series, and which can potentially obscure the signal of interest. This is especially important when using GPS to track processes that

have rates of only a few 0.1 mm/yr, such as is the case for monitoring sea level rise (Hammond et al., 2021).

Stochastic variation in GPS time series can be introduced at the processing stage of the GPS observations, such as mismodelling of the GPS orbits, atmospheric effects, and the satellite and receiver clocks (Ray et al., 2008; He et al., 2017). The environment around the GPS station can also be a source of stochastic variation in GPS time series, for example, from the monument the GPS antenna is attached to, the multipath around the station, vegetation cover, and mass loading from the atmosphere and hydrologic cycle. These sources of stochastic variation in the GPS time series can also have varying spatial scales. Errors introduced at the processing stage of GPS observations can introduce stochastic variation into all station time series, changes in hydrology produce variations seen from the continental to regional scale (Borsa et al., 2014; White et al., 2022), and noise related to GPS monuments only affects the individual station. Recent studies have shown that a significant portion of this spatially correlated variation in GPS time series can be attributed to atmospheric, oceanic, and hydrological mass loading (Klos et al., 2021; Gobron et al., 2021), which I collectively term surface mass loading in this thesis.

The goal of this thesis is to investigate the effect that surface mass loading has on the stochastic properties of GPS time series around the Great Lakes region of the U.S. and Canada. This region is ideal for studying these effects because it is covered by a dense network of long running GPS stations and it is known to be affected by significant hydrological loading due to water level changes in the Great Lakes. These water mass changes in the lakes can deform the region around the lakes by several millimeters (Argus et al., 2020; Xue et al., 2021; Wang et al., 2022). By using models to correct for the various surface mass loading effects, including the Great Lakes effect, I will investigate how the pattern of these stochastic variations changes in response to different mass loading processes. I will also investigate the stochastic properties of

the GPS stations with mass loading effects removed, in order to determine if there is a relationship between the GPS monument type and the noise characteristics of the time series.

The primary questions that will be addressed in this thesis are:

- What are the primary drivers of stochastic variation in GPS time series around the Great Lakes region?
- How do stochastic properties change when different surface mass loading models are applied, and how does this affect the rate uncertainty of stations?
- Does filtering the time series remove the need to correct for surface mass loading?
- Is there a relationship between monument type and the stochastic properties of GPS time series?

1.2 Background

1.2.1 Noise in GPS time series

Accounting for the stochastic properties of a GPS time series is critical when estimating station velocities with realistic uncertainties and determining whether subtle station motions are significant or not. Johnson and Agnew (1995) showed that assuming only white noise (WN) in the time series can lead to velocity uncertainties being severely underestimated if there is also long term temporally correlated noise in the observations. This temporally correlated noise is most often referred to as power law (PL) noise because its power, P, is proportional to its frequency raised to the power κ, $P \propto f^{\kappa}$, where κ is the spectral index of the noise. The spectral

index in most geophysical signals commonly falls between -3 and 1 (Johnson and Agnew, 1995), with it typically falling between -2 and 0 in GPS time series. A stochastic model of a combination of WN ($\kappa = 0$) plus flicker noise (FL; $\kappa = -1$) has generally been adopted as the ideal noise model for GPS time series (Williams et al., 2004), but recent studies have shown that the spectral index of PL noise can vary spatially (He et al., 2021). This indicates that the WN + FL model may not accurately capture all of the PL noise properties for some GPS stations, and consequently the velocity uncertainties would be underestimated for those stations.

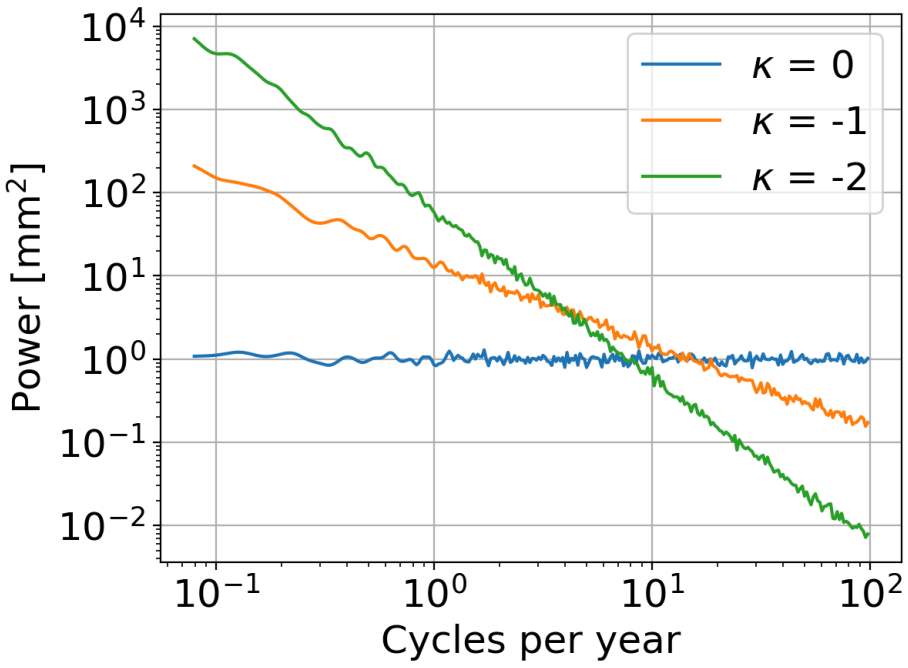

Figure 1.1: The effect of the spectral index on the power of the noise at different frequencies. 100 synthetic time series were generated for each spectral index and the Lomb-Scargle Periodograms of each averaged together to produce the plot above.

The effect of PL noise in the frequency domain of a GPS time series is an increase in the power of the noise at lower frequencies. This is demonstrated in Figure 1.1, which shows how random walk noise (RW; $\kappa = -2$), FL and WN are represented in the frequency domain of a time series. The RW dominates the lowest frequencies of the signal, while WN dominates the highest frequencies. This has an impact on the velocity uncertainty of the GPS time series, with WN being the major contributor to uncertainty for shorter time series, and PL noise with lower spectral indices contributing the most uncertainty for longer running time series (Figure 1.2). This means that the presence of PL noise with low spectral indices would be a limiting factor on the rate uncertainty, regardless of time series length.

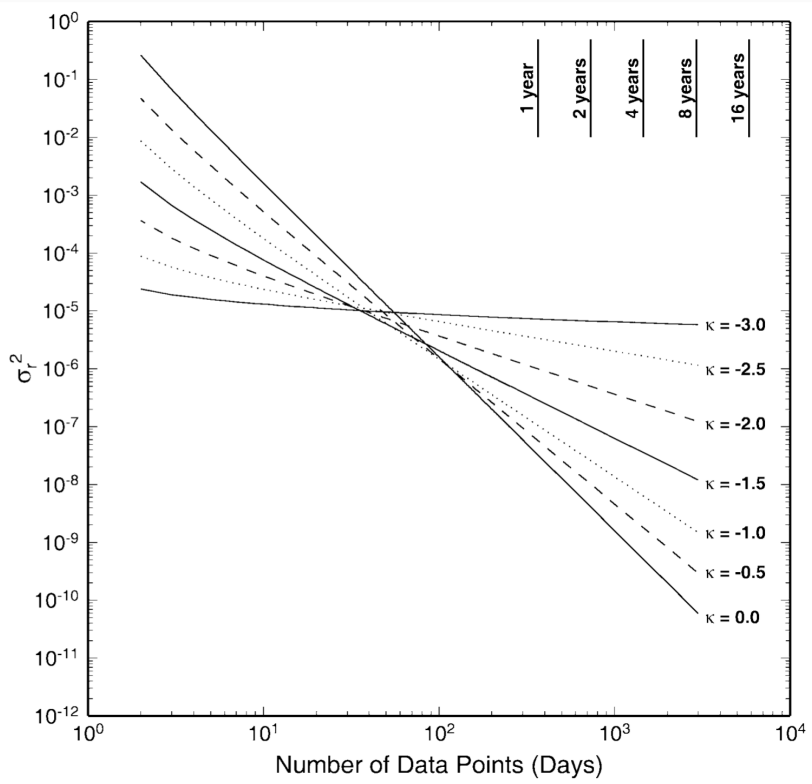

Figure 1.2: The effect of the spectral index and length of time series on the velocity uncertainty. From Williams (2003).

The optimal noise model for a GPS time series is still a matter of intense debate, with some alternative models being WN + FL + RW, WN + PL noise (i.e. allowing κ to vary), a Gauss-Markov process, or bandpass noise (Langbein, 2012; He et al., 2017; He et al., 2019; He et al., 2021). Previous studies have shown that it can be hard to distinguish between most of the noise models, particularly the WN + PL noise model and a WN + FL + RW model, but the choice of noise model can influence the estimates of velocity uncertainty (Langbein, 2012).

1.2.2 The common mode component and filtering

Much of the noise in GPS time series is spatially correlated as well as temporally correlated. The spatially correlated noise is often referred to as the common mode component (CMC) of the time series, and various filtering algorithms have been developed to remove the CMC (Wdowinski et al., 1997; Nikolaidis, 2002; Tian and Shen, 2016; Kreemer and Blewitt, 2021). Most of these filtering techniques work by "stacking" the time series, and they do not separate out the different signals mixed into the CMC. Dong et al. (2006) proposed an alternative approach using a principal component analysis (PCA) based method, in order to extract the different processing and environmental related errors into their respective components so that they can be interpreted.

The CMC is believed to be a combination of systematic errors from the GPS orbits, reference frame, and the processing of observations, as well as large scale environmental effects around the stations (He et al., 2017). An analysis of GPS time series after CMC filtering has shown a significant reduction in PL noise amplitude and in the estimated velocity uncertainty (Williams et al., 2004). However, there has not been much work into investigating the spatial distributions of stochastic properties before and after filtering, and whether correcting the time

series for surface mass loading before filtering can reduce PL noise amplitudes and rate uncertainty even further. This thesis will investigate the effectiveness of CMC filtering at removing surface mass loading from GPS time series. The CMC filtering algorithm used in this thesis, CMC Imaging (Kreemer and Blewitt, 2021), is outlined in Section 2.6.

1.2.3 GPS monuments

One potential source of stochastic variation in GPS time series is the monument type of the station. GPS stations can have a variety of monument types, some examples of which are steel or aluminum masts attached to buildings, steel pins attached directly to bedrock, concrete pillars with rods that extend a few meters into the ground, and deep-drilled braced monuments (DDBMs) which are anchored into the ground 10 or more meters and decoupled with the surface (Figure 1.3). One longstanding question in the geodetic community has been to what extent the different monument types influence the noise characteristic of the GPS time series.

Results from using a sensitive strainmeter showed that geodetic monuments largely exhibit RW characteristics (Wyatt, 1982; Wyatt 1989), meaning that monument instability could be a limiting factor on reducing long term GPS velocity uncertainties. An analysis of several GPS networks by Williams et al. (2004) determined that networks that primarily used DDBMs had the lowest RW noise content and velocity uncertainties, and these results have been confirmed in subsequent studies (Langbein, 2008; Langbein and Svarc, 2019). Compared to the Western U.S. where most of these monument comparisons have been carried out, the Great Lakes region has few DDBMs. The noise properties of the various monument types in this region will be investigated in this thesis.

Figure 1.3: An example of a deep-drilled braced monument, station P090 located in Reno, NV.

1.2.4 Surface mass loading

The elastic response of the Earth from surface mass loading is a known source of variation in geodetic time series (van Dam and Wahr, 1998). Mass loading can be generally split between loading that is tidal with a predictable period, and loading that is non-tidal or aperiodic. In daily GPS time series, the tidal loading effects are usually modeled and removed at the raw observation level before forming the daily solution, and will not be discussed further in this thesis. Non-tidal mass loading is attributed to atmospheric, oceanic and hydrological effects.

Atmospheric pressure loading is a significant source of scatter in GPS time series (van Dam and Herring, 1994; van Dam et al., 1994). It has a tidal component associated with diurnal

and semidiurnal pressure changes (Ray and Ponte, 2003), and a non-tidal component which is related to the passage of large scale pressure systems. Non-tidal atmospheric loading (NTAL) can cause surface displacements of 10 millimeters or larger (van Dam and Wahr., 1998). The magnitude of NTAL displacements increases towards the poles and away from coastal regions, where fluctuations in pressure from passing storm systems also have a larger magnitude (van Dam et al. 1994).

Non-tidal ocean loading (NTOL) is another significant contributor to variance in GPS time series, but its effect is confined to coastal regions. NTOL is caused by aperiodic mass redistribution in the ocean (van Dam et al., 2012). For instance, atmospheric pressure changes over the ocean can shift the weight of the water closer to land, causing coastal regions to deform. Displacements caused by NTOL can be up to 4-5 millimeters (Williams and Penna, 2011), less than the effect due to NTAL.

Fluctuations in groundwater, soil moisture and surface water all contribute to loading and deforming of the Earth's surface, and this deformation is observed in GPS time series (van Dam and Wahr, 1998; White et al., 2022). With the launch of the Gravity Recovery and Climate Experiment (GRACE) satellites in 2002, scientists have been able to study the temporal and spatial patterns in global terrestrial water storage (Tapley et al., 2004). Recently, combinations of GPS and GRACE data have been used to investigate higher resolution spatial and temporal changes in terrestrial water storage within watersheds (Argus et al. 2022). Displacements due to hydrological loading can be 10's of millimeters (Argus et al., 2020), and because water storage can change with annual to inter-annual periods, it can significantly bias GPS station velocity estimates (Santamaría-Gómez and Mémin, 2015). This makes it critical to correct for long term hydrological loading, as it can obscure other long term geophysical processes.

Recent studies have investigated the relationship between surface mass loading and the stochastic properties of GPS time series. He et al. (2017) showed that correcting for atmospheric, oceanic and hydrological loading can influence the best fitting stochastic model and change velocity uncertainty estimates. Li et al. (2018) used wavelet coherence to investigate the time variable phase between surface mass loading and the GPS time series in Eurasia, finding generally good agreement between the two, but also noting a decrease in the spectral index for some corrected time series. More recently, Gobron et al. (2021) looked at the effect of NTAL+NTOL (NTAOL) in a set of ~10,000 globally distributed stations, showing that WN amplitudes are underestimated at high latitudes in uncorrected time series. A study by Klos et al. (2021) looked at how surface mass loading affects station correlations for different frequency bands, finding that NTAOL is responsible for correlation between stations at all frequencies while hydrologic loading is responsible for correlation only at the lowest frequencies (i.e., annual to inter-annual). All of these studies highlight the importance of understanding surface mass loading and its effect on the estimation of velocity uncertainties. This thesis will expand upon these works by looking at a smaller region with a dense coverage of stations and a known significant source of surface mass loading, the Great Lakes. A detailed look at how the stochastic parameters of GPS time series vary with respect to known mass loading signals can then be had. Surface mass loading corrected time series will also be compared across monument types to see the extent that different monument types influence the stochastic properties of the time series.

1.2.5 The Great Lakes region

The Great Lakes of the Midwest U.S. is the largest group of freshwater lakes on Earth, covering an area of 244,000 km^2 and containing around a fifth of the world's unfrozen freshwater supply (U.S. Environmental Protection Agency and Government of Canada, 1995). Oscillations in the climate and hydrological cycle drive changes in the water levels of the Great Lakes, and recently there have been sustained periods of lower lake levels due to increased overlake evaporation, which are broken up with periods of rapid filling due to extreme precipitation (Norton et al., 2019). These variations in water levels are likely to continue since temperature is expected to increase and fluctuations in precipitation are predicted to become more extreme in the Midwest U.S. under human caused global climate change (Zhang et al., 2019).

GPS time series around the Great Lakes capture the loading and unloading of the Earth's surface due to water mass changes within the lakes. A study by Argus et al. (2020) showed that during the time period of 2012-2019, increased water volume in the lakes led to a subsidence of the lake bottoms by more than 20 millimeters. For stations next to or nearby the Great Lakes, the loading and unloading of the lakes will significantly contribute to the observed scatter and potentially bias the velocities of those stations (Xue et al., 2021; Wang et al., 2022).

Understanding how the Great Lakes loading and unloading impacts the station motions is especially important because the Great Lakes region is also undergoing glacial isostatic adjustment (GIA) from the unloading of the Laurentide Ice Sheet ~20,000 years ago (Dyke and Prest, 1987). GIA is a focus of intense study because it can inform us of the properties of the Earth's crust and upper mantle (Wu and Peltier, 1983), and is also a major contributor to sea level rise along the coasts (Peltier, 1999). GPS is a valuable tool for studying GIA (Peltier et al., 2015), but it is necessary to evaluate the impact of the Great Lakes loading, and other loading effects on station velocities and uncertainties in order to use it to its full potential.

Chapter 2: Data and Methods

2.1 GPS data

Daily position time series from 2,481 GPS stations for the time period 2005.0 to 2023.0 will be used in this study. The stations span the box defined by 36°N to 51°N and 97°W to 60°W. The distribution of stations densely covers the region from the Great Plains to the Atlantic Coast, with sparse coverage to the north of the Great Lakes (Figure 2.1). The average timespan of the station time series is ~10 years. The GPS data have been collected from a variety of networks, both public and private, and processed by the Nevada Geodetic Laboratory (NGL) for download on their website (http://geodesy.unr.edu/, Blewitt et al., 2018). Daily precise point position solutions are determined using the GipsyX version 1.0 software provided by the Jet Propulsion Laboratory (JPL), and positions are aligned to the IGS14 reference frame. More details on the processing strategy are provided on the NGL website (http://geodesy.unr.edu/gps/ngl.acn.txt). Only stations with time series spanning longer than 2.5 years will be considered, since it has been

shown that the velocity of shorter time series can be significantly biased by the seasonal signal (Blewitt and Lavallée, 2002).

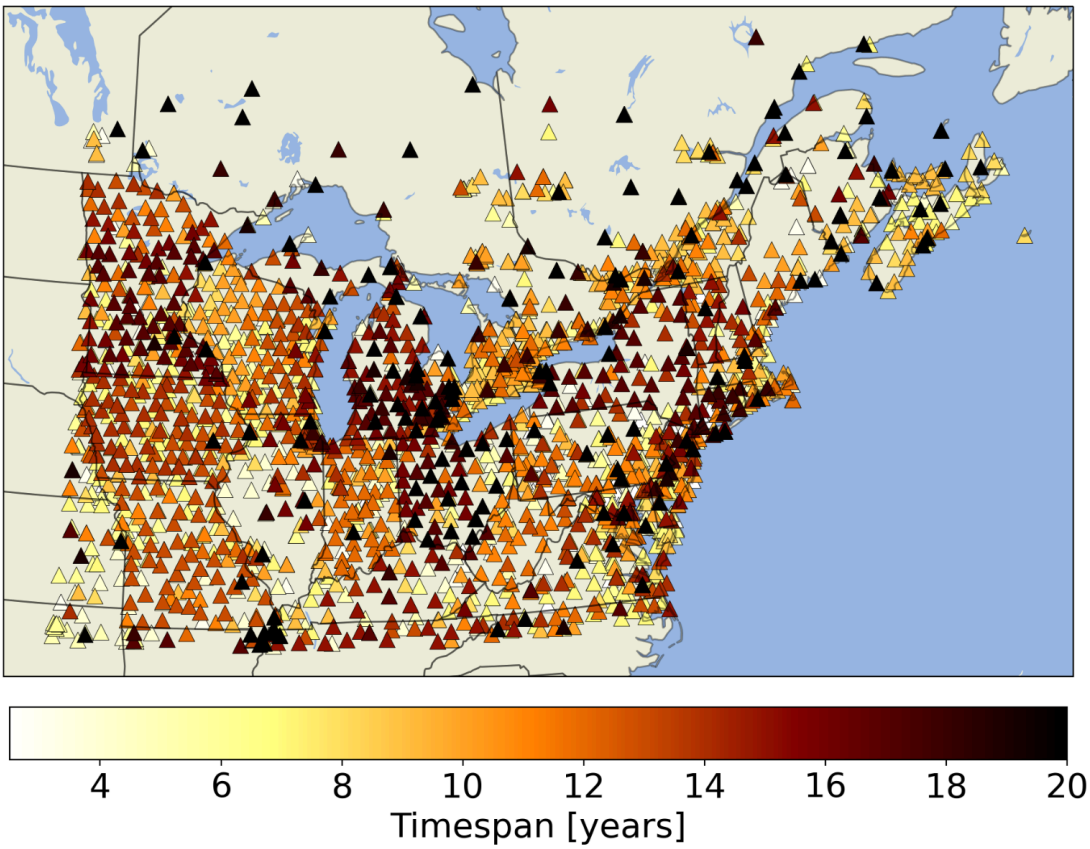

Figure 2.1: Map of data used colored by time series length in years.

2.2 NTAL, NTOL, and hydrological loading models

Models of NTAL and NTOL displacements are made available by the Earth System Modelling Group of the German Research Center for Geoscience (ESMGFZ) (http://rz-vm115.gfz-potsdam.de:8080/repository; Dill and Dobslaw, 2013) in 0.5° × 0.5° grids

with a 3 hour time interval. To get a prediction of loading displacement at each station, a daily average of the 3 hour NTAL and NTOL grids is produced and interpolated to station positions (Argus et al., 2022, Supplementary Information). I only use NTAL and NTOL together, which I will call the "NTAOL" model.

I also use models of predicted displacement due to hydrological mass changes. The GRACE "mascon" solutions solve for variations in the Earth's gravity field, which are related to variations in terrestrial water storage (Save et al., 2016). In this thesis, the predicted loading deformation from the GRACE mascons will be termed the "GRACE" model. Another hydrological loading model uses water level measurements from tide gauges in large artificial reservoirs and natural lakes, including the Great Lakes, in order to estimate water mass change and predict ground displacements. The model based on water level measurements will be termed the "LAKE" model. Predictions of surface deformation for both of these models is calculated using Green's functions for a spherical self-gravitating Earth with an assumed PREM structure (Argus et al., 2017). Both GRACE and LAKE models have a monthly resolution, and are interpolated to the GPS station locations and observation times. More details on the calculation of these loading models can be found in the supplementary information of Argus et al. (2022).

The displacement corrections for each station are available in the TENV3 format station position files provided on the Nevada Geodetic Laboratory webpage (http://geodesy.unr.edu/gps_timeseries/tenv3_loadpredictions/).

In this thesis I will produce solutions that are uncorrected, corrected for NTAOL (NTAL+NTOL), corrected for NTAOL+GRACE, and corrected for NTAOL+LAKE. The vertical component variance of each model is shown in Figure 2.2.

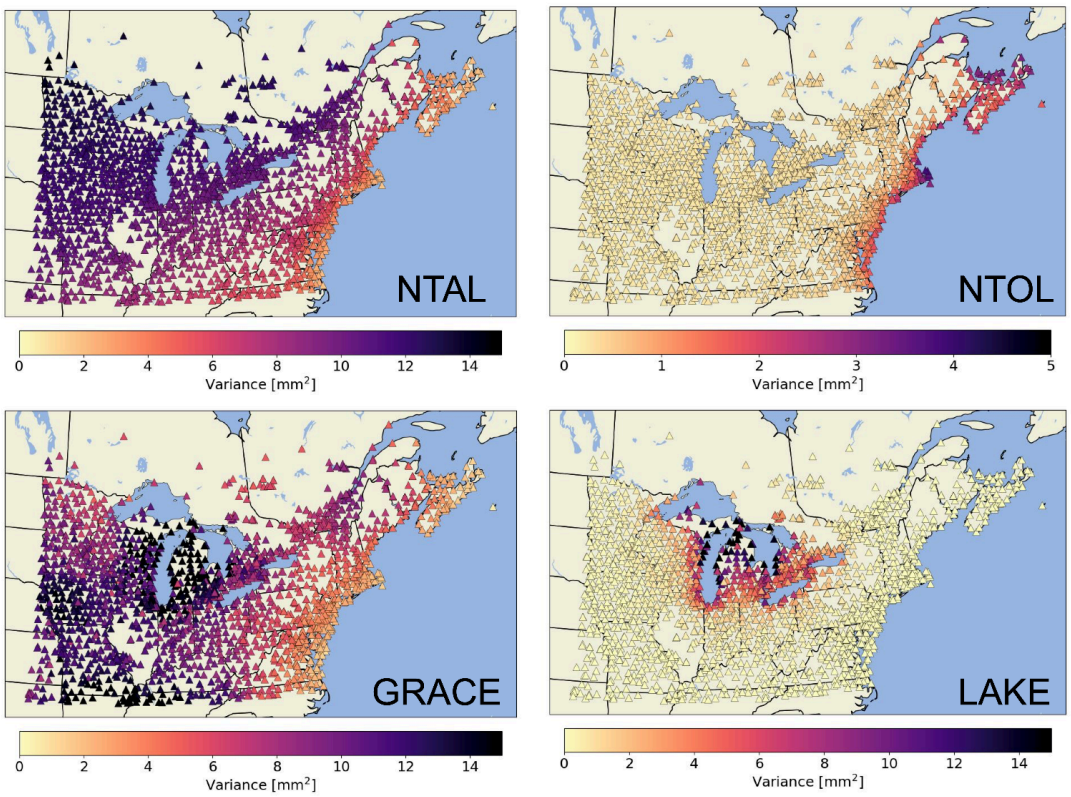

Figure 2.2: Variance of the vertical component of the different loading models used in this study.

2.3 Station monument metadata

Monument information from station site logs is now available on the NGL website located at http://geodesy.unr.edu/monuments/MonumentTable.txt. Not every station in the study region has monument information. I augment the information in the NGL Monument Table with monument information for stations operated by the Wisconsin Department of Transportation (https://wisconsindot.gov/Pages/doing-bus/eng-consultants/cnslt-rsrces/tools/wiscors/stations.aspx). In total, 831 stations in the study region have information on monument type. The monument information in site logs is not standardized, so I went through each of the 831 stations and classified the monument type into one of five categories: DDBMs, roof mounted, concrete pillars,

steel towers, and any monument directly attached to bedrock. To do this, I used information contained in the augmented monument table and then verified this information with pictures of the station if available. I end up with 11 DDBMs, 461 roof mounted, 314 concrete pillars, 33 steel towers and 12 stations attached to bedrock.

2.4 GPS time series fitting

The deterministic behavior of a GPS time series can be modeled as a function of time, t:

$$y(t) = y_0 + vt + \sum_{i=1}^{2}[(a_i \sin(2i\pi t) + b_i \cos(2i\pi t)] + \sum_{i=1}^{k} c_i H(t_i)$$

Where y_0 is the intercept, v is the velocity, a_i and b_i i = 1, 2 are the annual and semi-annual seasonal terms, and the last term adds an offset of of size c_i at time t_i with the Heaviside step function $H(t_i)$ for i = 1,...,k steps.

Weighted least squares is used to solve for these deterministic parameters, the solution of which is given by:

$$\hat{x} = (A^T C^{-1} A)^{-1} A^T C^{-1} y$$

Where A is the design matrix for the regression, C is the covariance matrix of the observations, and the estimated parameters are $\hat{x} = [y_0, v, a_1, b_1, a_2, b_2, c_1, \ldots, c_k]^T$.

Residual time series, $\hat{r}$, can then be computed be the equation:

$$\hat{r} = [I - (A^T C^{-1} A)^{-1} A^T C^{-1}]\, y = y - A\hat{x}$$

Where I is the identity matrix. An example of a time series fit can be seen in Figure 2.3.

To prevent biases in the parameter estimation, after an initial fit the residual time series are carefully inspected to detect previously unknown offsets, periods of increased noise amplitudes, and nonlinear motion. Stations that exhibit extreme irregular movement (e.g. from equipment failure, station relocation, etc) are considered to not reflect actual ground motion, and are removed from this analysis. The deterministic model parameters are then once again estimated using an updated list of offsets and excluded stations. Residual positions that are >3σ deviations are flagged as outliers and removed from the residual time series, and this process is repeated iteratively until no outliers are identified.

In a slight modification to the least squares solution above, damped least squares with a damping parameter λ, which can be more robust than just weighted least squares. The solution is given by $\hat{x} = (A^T C^{-1} A + \lambda I)^{-1} A^T C^{-1} y$.

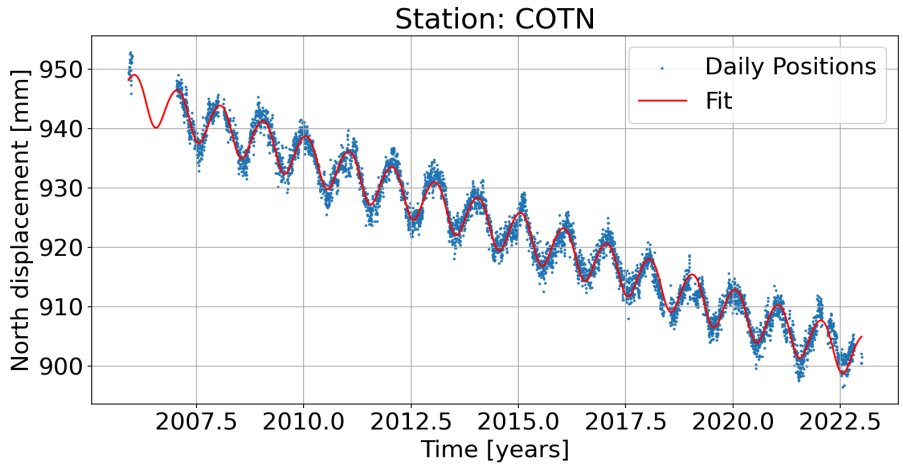

Figure 2.3: An example of a damped least squares fit to the north component of the station COTN in northern Minnesota.

2.5 Estimating noise amplitudes with LS-VCE

For this analysis I am choosing the WN + FL + RW model to represent the stochastic behavior of the GPS time series. This model has been shown to be similar to the WN + PL model, but has more conservative estimates on velocity uncertainty (Langbein, 2012).

To determine the stochastic parameters of the residual time series, I used the multivariate version of the Least Squares - Variance Component Estimation (LS-VCE) (Amiri-Simkooei, 2008). I use LS-VCE to determine the amplitudes of WN, FL and RW in the multivariate residual time series (i.e. using the east, north and up components together). Furthermore, I apply a non-negative constraint (Amiri-Simkooei, 2016) when negative amplitudes are encountered, which is not a realistic scenario. I only estimate stochastic parameters for stations that have 1,500 or more observations, to ensure that the estimates are robust.

The stochastic model of daily positions can be modeled as the covariance matrix:

$$\mathbf{C} = \sigma_{\mathbf{wn}}^{\mathbf{2}}\mathbf{I} + \sum_{\mathbf{i=1}}^{\mathbf{k}} \sigma_{\mathbf{i}}^{\mathbf{2}}\mathbf{Q_i}$$

Where **I** is the identity matrix, σ_{wn} is the amplitude of the WN variance component, σ_i with i = 1,..,k are the amplitudes of the other variance components, and $\mathbf{Q}_i$ with i = 1,...,k are the cofactor matrices that represent temporally correlated covariances in the time series. The variance components can then be estimated in the least squares paradigm with the solution given by $\hat{\sigma} = N^{-1}l$, where

$$N_{ij} = \frac{1}{2}trace(Q_i C^{-1} P_A^{\perp} Q_j C^{-1} P_A^{\perp})$$

and

$$l_i = \frac{1}{2} trace(\widehat{R}^T C^{-1} Q_i C^{-1} \widehat{R})$$

$\widehat{R}$ is the multivariate residual time series given by the east, north and up component residual time series as determined in Section 2.4, and $P_A^{\perp} = [I - (A^T C^{-1} A)^{-1} A^T C^{-1}]$ is the projection matrix. The cofactor matrices representing FL and RW are constructed according to Williams (2003).

One thing to note is that independence was assumed between the 3 components of the residual time series. This reduces the estimate of the multivariate variance components to an average of the 3 time series components. If there is correlation between the components, then this would not be the case. The LS-VCE framework makes it easy to estimate the covariance matrix for the 3 components, but I have chosen to assume independence between the components in order to simplify the analysis and reduce the computation time. This decision is justified by the results of Amiri-Simkooei (2008), which showed insignificant correlation between the 3 time series components.

2.6 Filtering with CMC Imaging

Common mode component (CMC) Imaging is a robust method for estimating the spatially correlated signal in GPS time series. The details of how CMC Imaging works is provided in Kreemer and Blewitt (2021), but a basic outline of the procedure is as follows:

1. Compute residual time series for each station by removing the fitted deterministic model as outlined in Section 2.4

2. Calculate a correlation coefficient for each pair of stations. The correlation coefficient is based on the median absolute deviation (MAD), and this MAD-based correlation coefficient is defined in Kreemer and Blewitt (2021).
3. For each station, fit a line to the correlation coefficient and distance with every other station. Save the slope and intercept of this fitted line.
4. Use Delaunay triangulation to connect every station.
5. Construct the CMC for every epoch of the station time series by using a weighted median of the connected station residuals, plus every other station residual within the median distance of the connected stations. The weight assigned to each filter station is based on the predicted correlation coefficient using the slope and intercept determined in Step 3, and the formal uncertainty of the observation.

CMC Imaging is an iterative approach that requires using the longest running and most complete station time series to first de-bias the trend in less complete stations, before the CMC can be computed for every station. However, in comparison to other filter methods, it allows almost every station to act as a filter station, and is capable of capturing both local and regional scale effects. In comparison to PCA-based filtering methods, CMC Imaging does not separate out the different components in the CMC. An example of a CMC Imaging filtered time series is shown in Figure 2.4.

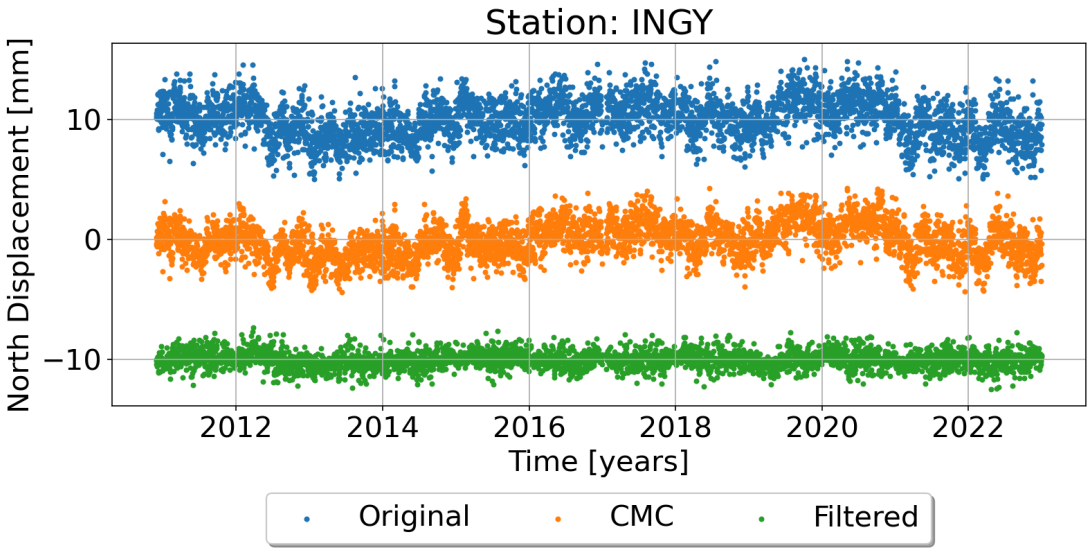

Figure 2.4: Example of a CMC Imaging filtered time series. CMC Imaging captures much of the broad scale and locally correlated signal in the CMC and removes it from the time series. The station is located on the southern shore of Lake Michigan.

2.7 Data preparation

All the loading enhanced tenv3 format stations files for the study region are downloaded from http://geodesy.unr.edu/gps_timeseries/tenv3_loadpredictions/. Stations with a timespan less than 2.5 years are excluded from the analysis. Then 4 different sets of time series are made by subtracting (or not subtracting) the loading models that are contained within the enhanced tenv3 files: uncorrected, NTAOL corrected, NTAOL+GRACE corrected and NTAOL+LAKE corrected. The processing of each set of time series is then:

1. Estimate a fit to the deterministic model as outlined in Section 2.4 and remove the fit from the raw time series to produce residual time series.
2. Perform outlier detection, and repeat steps 1 and 2 until no more outliers are detected.

3. Carefully inspect the residual time series and document any jumps or non-linear motion.
4. Repeat steps 1 - 4 until all jumps that can be visually identified are corrected, and stations that have extreme non-linear motion are excluded.
5. Perform CMC Imaging as outlined in Section 2.6.
6. Estimate fit to filtered time series and produce CMC filtered residual time series.
7. Carefully inspect CMC filtered residual time series for more jumps and repeat steps 1 - 6 until all jumps in the filtered time series are corrected.
8. Calculate stochastic parameters according to Section 2.5 for unfiltered and CMC filtered time series.

This produces residuals and estimated stochastic parameters for the unfiltered and CMC filtered time series of the 4 different loading corrected (or uncorrected) sets mentioned above. It is very likely that some jumps were missed during visual inspection given the size of the dataset, and this will influence the RW amplitudes for stations that have these undetected jumps.

Chapter 3: Results

In this chapter I will compare uncorrected and surface mass loading corrected GPS time series using 4 metrics: variance reduction in corrected residual time series; white noise, flicker noise and random walk noise amplitudes; velocity uncertainties; and average power spectrum of residual time series. I will also compare unfiltered time series to CMC filtered time series to evaluate the improvement gained by filtering and the extent to which surface mass loading is removed in the filtering process. Finally, I compare noise amplitudes and velocity uncertainties of GPS stations grouped by monument type to investigate the role it has on the stochastic variability of the time series.

3.1 Contributions of loading components

To assess the contribution of each loading component, I calculate the variance reduction from applying the loading model to the GPS time series. Variance reduction is defined as:

$$\text{Variance Reduction} = 100\% \times \frac{var(GPS) - var(GPS-LOAD)}{var(GPS)}$$

In this case, a positive value indicates a decrease in variance while a negative value indicates an increase in variance.

Figure 3.1 shows the variance reduction after correcting for the different loading models. Note that the variance reduction for GRACE and LAKE corrections show the additional improvement when applying those loading models to the NTAOL corrected time series. All loading corrections have a greater variance reduction in the vertical component of the time series compared to the horizontal components. For NTAOL corrections the average improvement in the east, north and vertical components is 7.3%, 4.6% and 33.3% respectively. The average additional improvement of GRACE in the east, north and vertical components is -0.3%, 2.4% and 17.2%, respectively. LAKE corrections will be discussed in Section 3.5.

The effect of correcting for surface mass loading is not evenly distributed. NTAOL has the strongest effect in the north and inland region of the study area, where the fluctuations in atmospheric pressure are greatest. GRACE has the strongest effect around the Great Lakes and in the Upper Midwest, which corresponds to the hydrology and climate of the region. There is also some negative improvement (i.e. increase in variance) observed when correcting the east component of the time series with GRACE, which is most apparent in the eastern portion of the study region. Overall the magnitude of GRACE corrections for the horizontal components is very small, and they may not accurately capture the magnitude of horizontal motions due to hydrological loading (see Section 4.2).

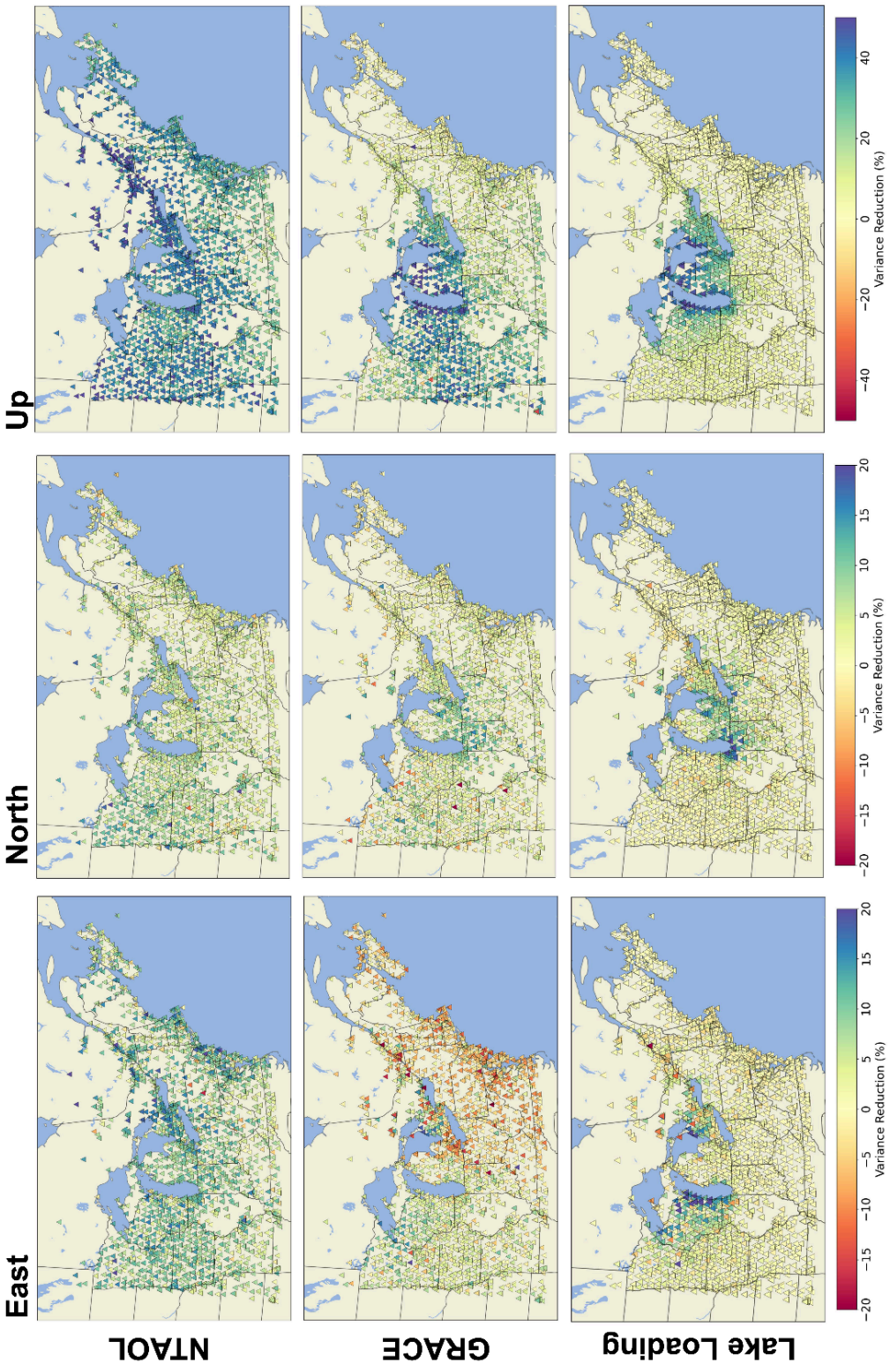

Figure 3.1: Variance reduction from applying the loading corrections.

When only considering the observed scatter in GPS time series, NTAOL explains the largest proportion of the scatter compared to hydrological loading. However, hydrological loading has a much stronger effect on the station velocities. Differences in station vertical velocities between NTAOL corrected and NTAOL+GRACE corrected time series is shown in Figure 3.2. The velocity differences can be greater than 1 mm/yr around the Great Lakes and the Upper Midwest. The sign of the velocity change around the Great Lakes is highly dependent on the timespan of the individual stations, with stations that span the full 2005.0 to 2023.0 time period largely showing a positive velocity difference, while the velocity change for stations only spanning a portion of the time period may be positive of negative depending on the time period they are active.

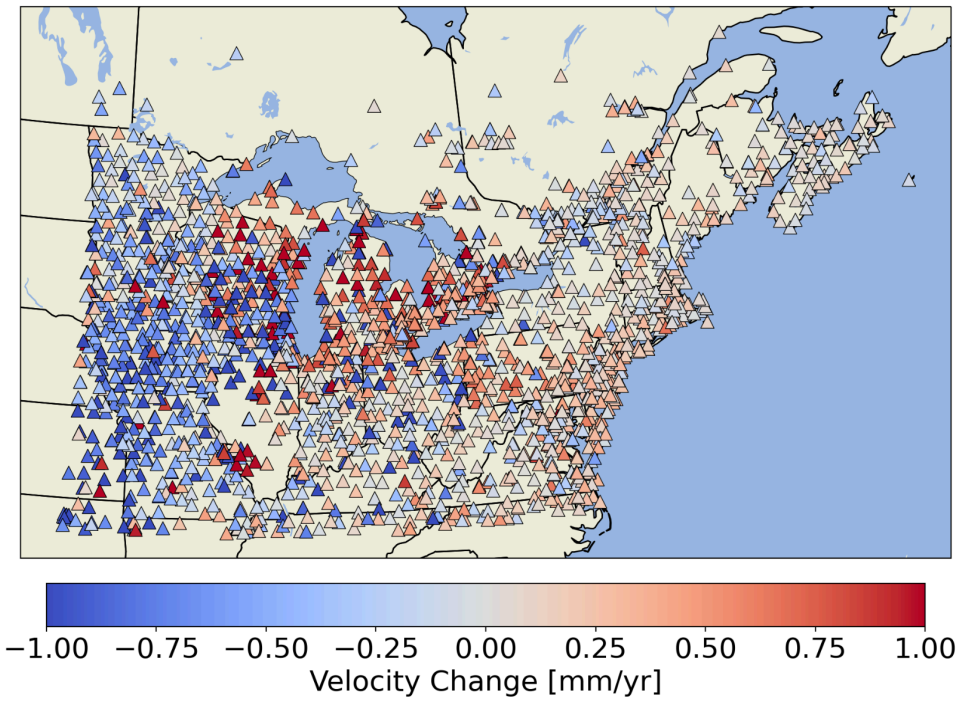

Figure 3.2: Vertical velocity differences after applying the GRACE correction.

3.2 Spatial variation of stochastic properties

Table 3.1: Median noise amplitudes and velocity uncertainty of uncorrected, corrected and filtered time series. The solution type indicates what loading models the time series have been corrected with.

*CMC filtered time series have been corrected for NTAOL+GRACE prior to filtering.

Solution	WN Amplitude [mm]	FL Amplitude [mm/yr^(1/4)]	RW Amplitude [mm/yr^(1/2)]	Uncertainty [mm/yr]
Uncorrected	1.52	9.75	0.00	0.35
NTAOL	1.81	4.90	0.76	0.38
NTAOL+GRACE	1.80	4.77	0.00	0.18
CMC Filtered*	1.37	1.92	0.38	0.16

Stochastic properties of the multivariate residual time series are estimated using LS-VCE, as outlined in Section 2.5. Only stations that have more than 1,500 observations are used. Table 3.1 summarizes the results with the median value of WN, FL, RW and velocity uncertainties for all stations after applying the different loading models.

Figure 3.3 shows the spatial patterns of WN, FL and RW amplitudes of the uncorrected (top row) and NTAOL+GRACE corrected time series (bottom row). Figure 3.4 shows the differences in the WN, FL, and RW amplitudes after correcting for NTAOL (bottom row), and the additional differences from the NTAOL corrected time series when correcting with GRACE (top row). Both figures 3.3 and 3.4 show that correcting for NTAOL increases both WN and RW amplitudes in some stations. This is especially true in regions where NTAL has the highest variance (Figure 2.2). These results are consistent with the masking effect of NTAOL on WN seen by Gobron et al. (2021). The additional correction with GRACE to the time series only

affects RW amplitudes significantly, with RW amplitudes decreasing most noticeably around the Great Lakes and in the Upper Midwest (Figure 3.4).

After correcting the time series for NTAOL+GRACE, the WN and FL amplitudes show little spatial variability throughout the study region, in contrast to the uncorrected time series. WN and FL have median values of 1.8 mm and 4.8 mm/yr$^{1/4}$, respectively, in the corrected time series, compared to 1.5 mm and 9.8 mm/yr$^{1/4}$ in the uncorrected time series. The RW amplitudes in the NTAOL+GRACE corrected time series increase to an average value of 0.5 mm/yr$^{1/2}$ from almost no RW in the uncorrected time series, but the median value is still 0.0 mm/yr$^{1/2}$. RW in the corrected time series is also highly spatially variable, with higher RW amplitudes visible in some state networks, in particular Wisconsin and Minnesota.

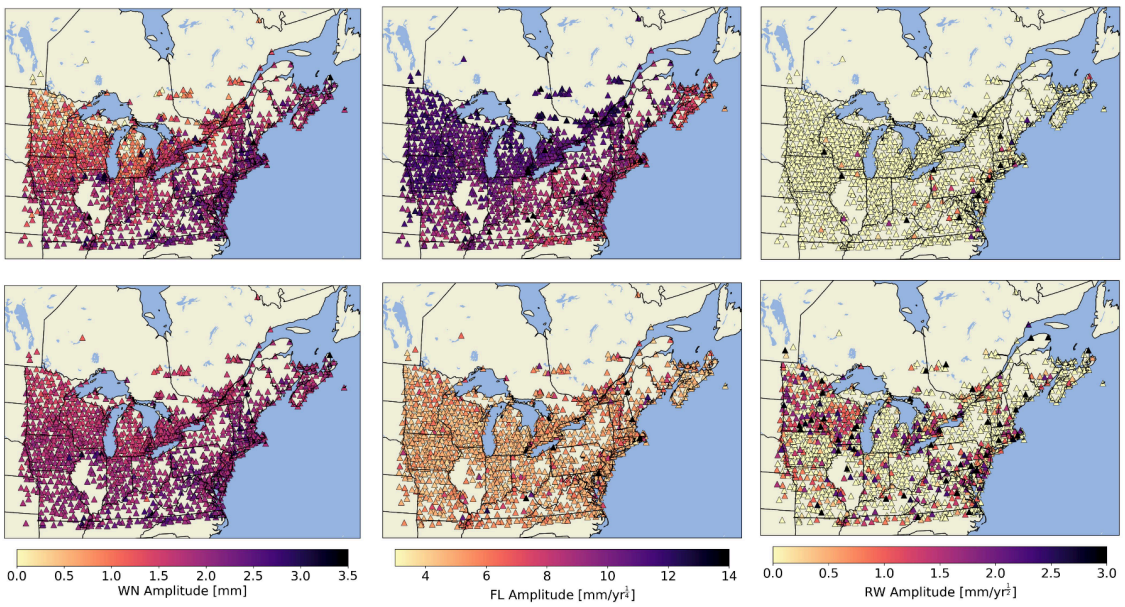

Figure 3.3: (Top) WN, FL, and RW amplitudes in uncorrected time series. (Bottom) WN, FL, and RW amplitudes in NTAOL+GRACE corrected time series.

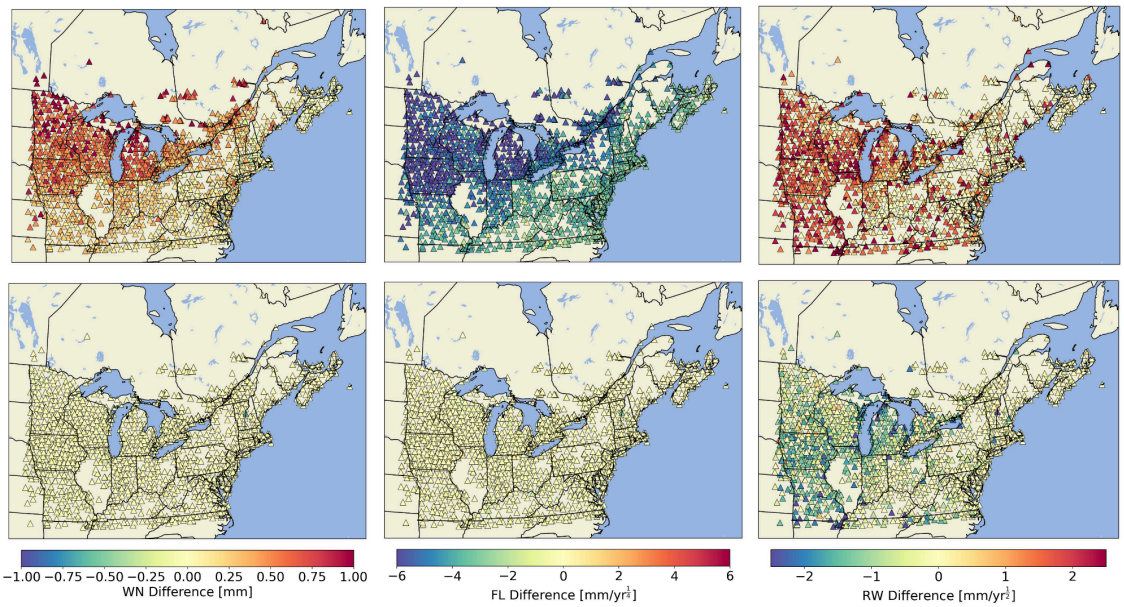

Figure 3.4: (Top) Differences in WN, FL, and RW amplitudes between uncorrected and NTAOL corrected time series. (Bottom) Differences in WN, FL, and RW amplitudes between NTAOL corrected and NTAOL+GRACE corrected time series.

I estimate the velocity uncertainty for each station in order to compare the total effect of the stochastic properties on the time series. The velocity uncertainties are calculated using the noise model defined in Section 2.5, so that temporal correlations in the noise are considered. Uncertainties are calculated at the time of estimating the stochastic parameters through the multivariate LS-VCE, but instead of estimating the actual velocity uncertainties which are also representative of the time series length, I estimate the velocity uncertainties for a time series length of 8 years and no missing observations, which is a best case scenario. This is done so that differences in velocity uncertainties only represent differences in the stochastic properties of the time series, and I can directly compare velocity uncertainties to surrounding stations. Since I use the multivariate time series to estimate the stochastic properties, the 8-year velocity uncertainties represent an average of the 3 time series components.

Figure 3.5 shows the 8-year velocity uncertainties for the uncorrected (Top) and the NTAOL+GRACE corrected (Bottom) time series. Velocity uncertainties for the uncorrected time series increase slightly with the magnitude of the NTAOL effect, and do not have a large variation throughout the study region. Uncertainties in the NTAOL+GRACE corrected time series are much lower, but for some stations the uncertainties increase with a corresponding increase in the RW amplitudes. Similar to the map of RW amplitudes in the NTAOL+GRACE corrected time series, the pattern of velocity uncertainties seems to be dependent on the state network. This could indicate potential systematic errors within some of the state networks.

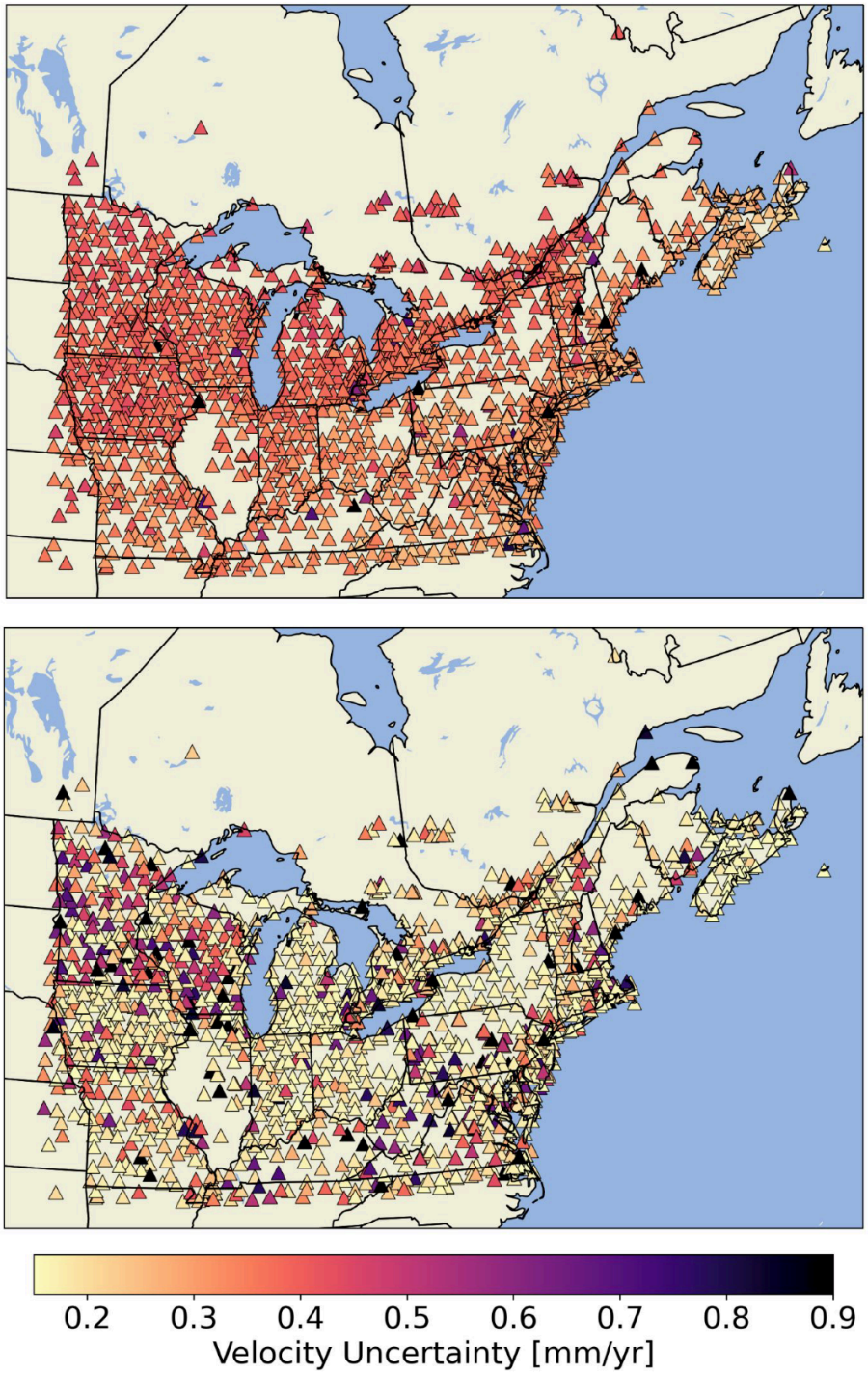

Figure 3.5: Velocity uncertainties for a time series length of 8 years with no missing observations. (Top) Velocity uncertainties for the uncorrected time series. (Bottom) Velocity uncertainties for the NTAOL+GRACE corrected time series.

3.3 Power spectrum of the vertical residual time series

I use the Lomb-Scargle periodogram (Lomb, 1976; Scargle, 1982) to compare the power spectrums of the uncorrected and corrected residual time series. Figures 3.6, 3.7, and 3.8 show the average power spectra for uncorrected, NTAOL corrected, and NTAOL+GRACE corrected, respectively, of the vertical component residual time series. I do not show the horizontal components, because there is very little difference between the uncorrected and corrected power spectra for the horizontal residual time series. All power spectra show dips in the power consistent with the annual and semi-annual terms taken up in the deterministic model. Other periodic signals commonly seen in GPS time series appear as peaks in the power spectrum, namely the periods associated with the GPS draconitic year and its harmonics (Ray et al., 2008). The GPS draconitic signal is particularly hard to remove since it has a period of 351.2 days, close to the annual signal with a period of 365.25 days. While other studies have removed these other periodic signals (Gobron et al., 2021), I have not attempted to do so in this study.

Correcting for NTAOL significantly flattens the higher frequency portions of the power spectrum of the residual time series (Figure 3.7). The lower frequency portion of the average power spectrum is unaffected by NTAOL, and the slope of the lower frequency spectrum becomes steeper, consistent with an increase in the RW magnitudes observed in Figure 3.4. There is also a decrease in the power of the visible peaks with 10 or more cycles per year, possibly indicating these periods are associated with NTAOL in the GPS time series around the Great Lakes.

Time series that have been corrected with both NTAOL and hydrological loading from GRACE show a decrease in the power at lower frequencies and flattening of the slope, which is also consistent with a decrease in RW seen in the GRACE corrected time series. There is also a noticeable decrease in a peak seen in the power spectrum at 0.2 cycles per year, which could be

related to interannual cycles in hydrology in the Great Lakes region (Wang et al., 2022). Seen in both the NTAOL and NTAOL+GRACE corrected power spectra is a broad peak around 66.4 cycles per year. This has been noted in previous studies, and is believed to be related to the PPP processing strategy (Amiri-Simkooei et al., 2017; Gobron et al., 2021).

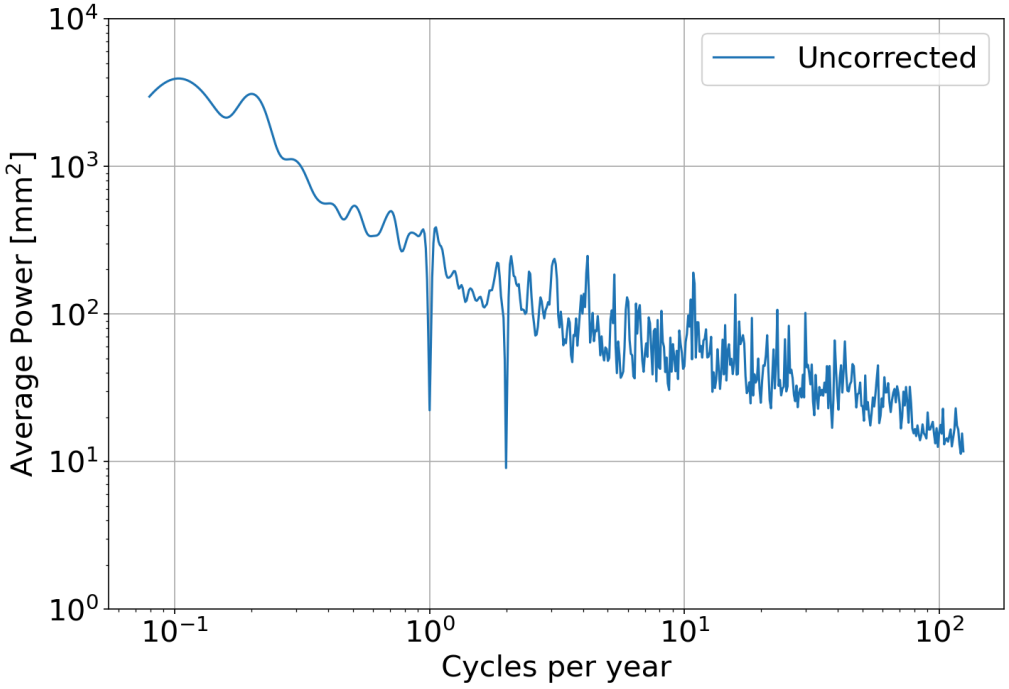

Figure 3.6: Average Lomb-Scargle periodogram for the vertical component of the uncorrected residual time series.

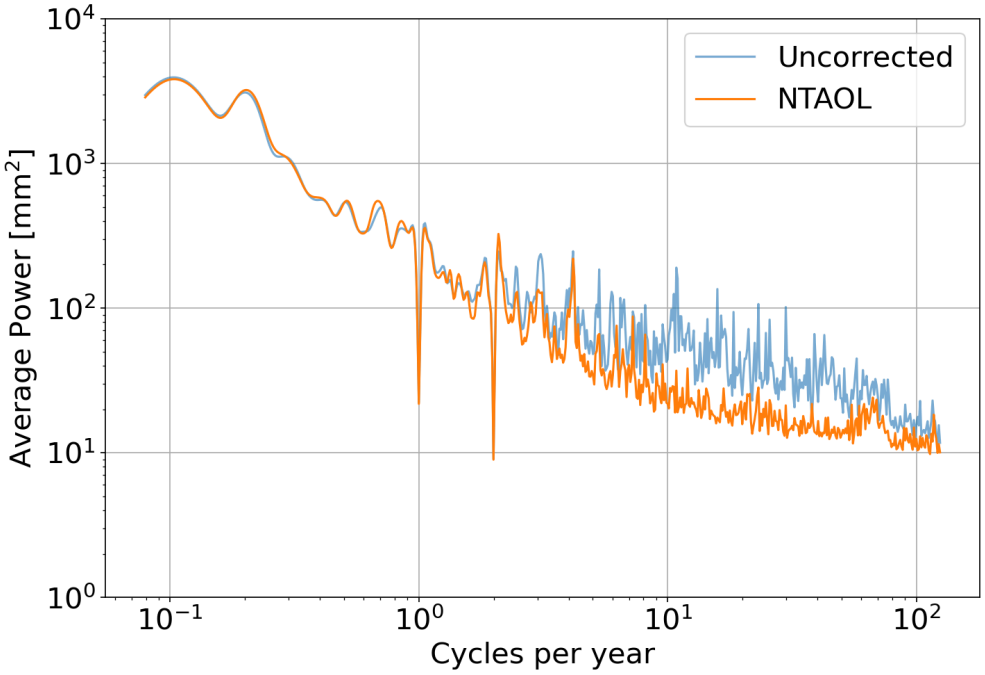

Figure 3.7: Same as Figure 3.6 but for the NTAOL corrected time series.

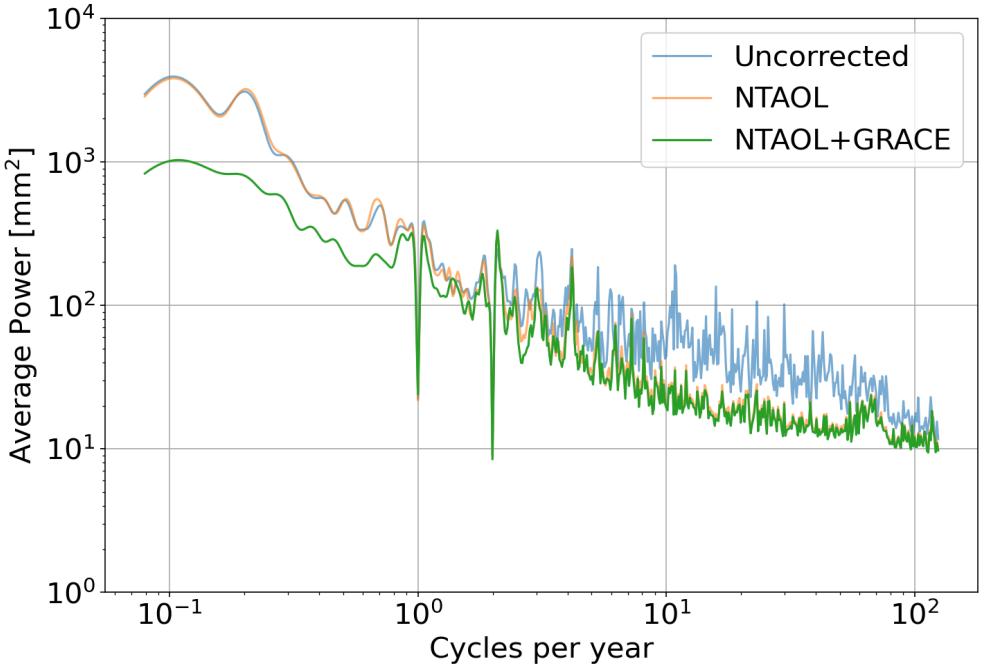

Figure 3.8: Same as Figure 3.6 but for the NTAOL+GRACE corrected time series.

3.4 CMC filtering

CMC Imaging (Section 2.6) is used to filter the time series. Figure 3.9 shows the variance reduction between NTAOL+GRACE corrected time series and the same time series but CMC filtered. Variance reduction is significant for every component, with reductions of 64.1%, 62.6% and 52.1% in the east, north and vertical components, respectively. Even higher variance reductions of 75-85% are concentrated around the Great Lakes and Upper Midwest, suggesting that there may be additional hydrological loading removed from the time series that is not accounted for in the GRACE model. There is also a region of significant variance reduction along the Mid-Atlantic Coast, possibly indicating some other regional effect that is not accounted for in any of the loading models.

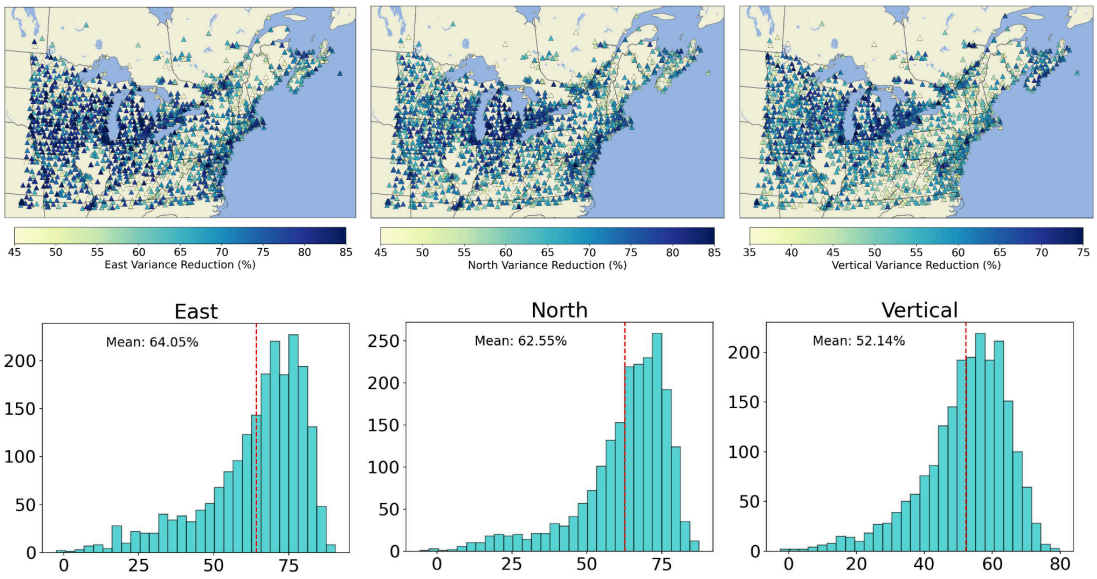

Figure 3.9: (Top) Variance reduction from CMC filtering, all time series are corrected for NTAOL+GRACE before filtering. (Bottom) Histograms of variance reduction from CMC filtering.

Next I look at how the stochastic properties change in CMC filtered time series. For these comparisons I only look at the differences between unfiltered and filtered time series that have been corrected with NTAOL+GRACE. Figure 3.10 shows how the WN, FL, and RW amplitudes change with filtering. Both WN and FL amplitudes decrease in almost every station. This indicates that some of the WN in the GPS time series is possibly due to systematic processing errors or errors within the GPS system itself, since WN is unlikely to be due to loading effects. FL is probably due to both processing and environmental related effects. Average RW amplitudes increase after CMC filtering, suggesting there is additional masking of RW amplitudes by the other noise components.

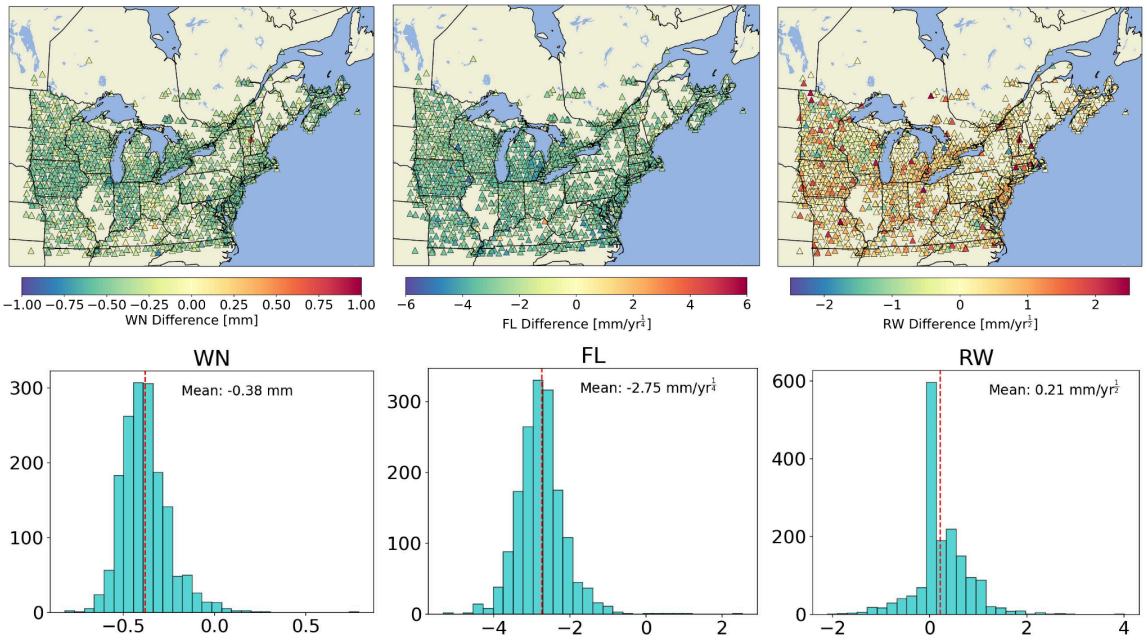

Figure 3.10: (Top) Difference in estimated stochastic parameters between unfiltered and CMC filtered time series. All time series have been corrected for NTAOL+GRACE before filtering. (Bottom) Histograms of differences.

Figure 3.11 shows the 8-year velocity uncertainties in the filtered NTAOL+GRACE corrected time series and the histogram of the differences from the unfiltered NTAOL+GRACE corrected time series. The velocity uncertainties are mostly influenced by the RW amplitudes, and 17.5% of stations have an increase in velocity uncertainty greater than 0.1 mm/yr. Compared to Figure 3.2, the velocity uncertainty dependence on the state/province network is less pronounced, but some states/provinces still appear to have considerably lower overall uncertainties (e.g. Michigan, New York and Nova Scotia).

I compare the average Lomb-Scargle periodogram of the unfiltered and filtered vertical residual time series (Figure 3.12). The CMC filtered residual time series have significantly less power at all frequencies, and is noticeably smoother at the higher frequencies. Many of the peaks associated with cycles of 6 times a year or more are reduced, but peaks at 3, 4 and 5 cycles per year are more pronounced. The broad peak associated with 66.4 cycles per year is still present, suggesting that the cause is not spatially correlated.

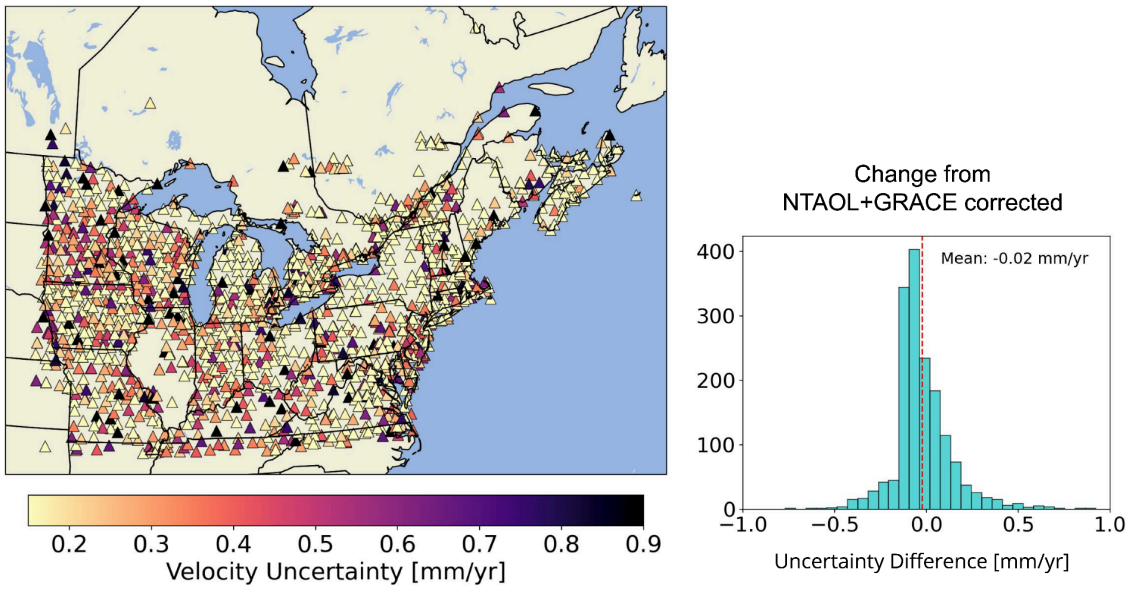

Figure 3.11: (Left) 8-year velocity uncertainties in CMC filtered NTAOL+GRACE corrected time series. (Right) Histogram of uncertainty differences between unfiltered and filtered time series.

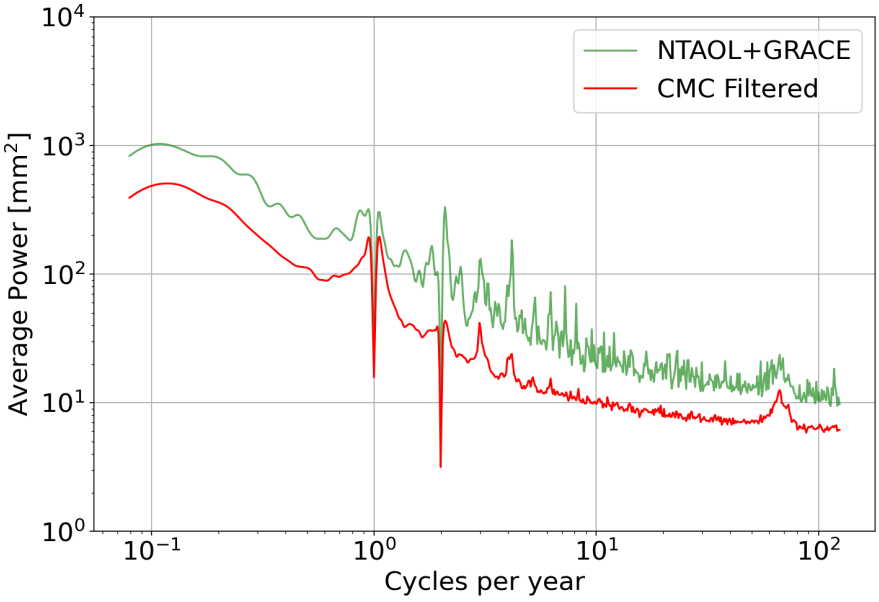

Figure 3.12: Average Lomb-Scargle periodogram of the vertical component of unfiltered and CMC filtered time series.

To see if there is any additional improvement gained by correcting time series before filtering, I compared uncorrected and loading corrected time series that have both been CMC filtered. Figure 3.13 shows the histograms of variance reduction between the filtered uncorrected time series and the filtered NTAOL+GRACE corrected time series. Variance reduction is 0.8%, 0.2% and 2.8% for the east, north and vertical components, respectively. There are no coherent spatial patterns in the variance reduction and maps of the variance reduction are not shown. It should also be noted that in filtered time series even small shifts in variance could lead to a large change in variance reduction %, since the overall variance is much less than for unfiltered time series. These results show that the CMC Imaging method is very effective at capturing the variance due to these mass loading signals.

Velocity differences between CMC filtered uncorrected time series and CMC filtered NTAOL+GRACE corrected time series were also looked at. Figure 3.14 shows the velocity differences for the vertical component. Unlike the results from the variance reduction comparison, here there is a clear difference when correcting for NTAOL+GRACE. While the CMC Imaging algorithm uses the longest running and most complete stations to debias the velocity estimates in shorter time series, it does not correct for the long term trend from hydrological loading. Since the long term trend from hydrological loading in the study region is mostly subsidence, correcting the stations with GRACE leads to an increase in their vertical velocity. However, it appears that CMC Imaging is very effective at debiasing the shorter time series, since much of the scatter seen in Figure 3.2 is removed. There are also slight velocity differences seen in the horizontal components, but for simplicity only the vertical component is shown.

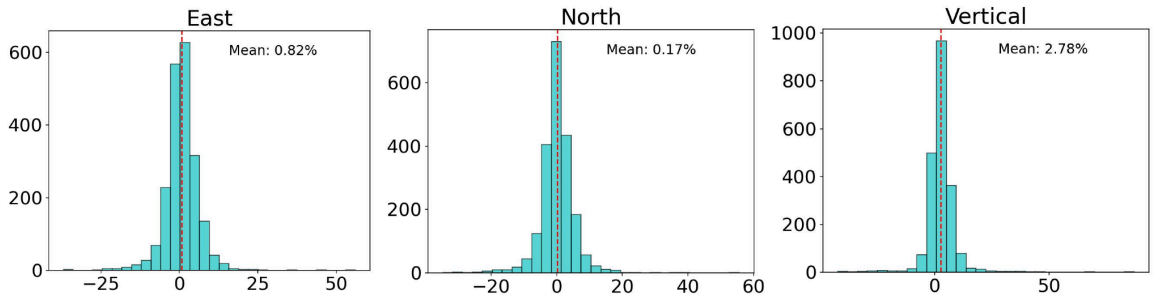

Figure 3.13: Histograms of variance reduction between CMC filtered uncorrected time series and CMC filtered NTAOL+GRACE corrected time series.

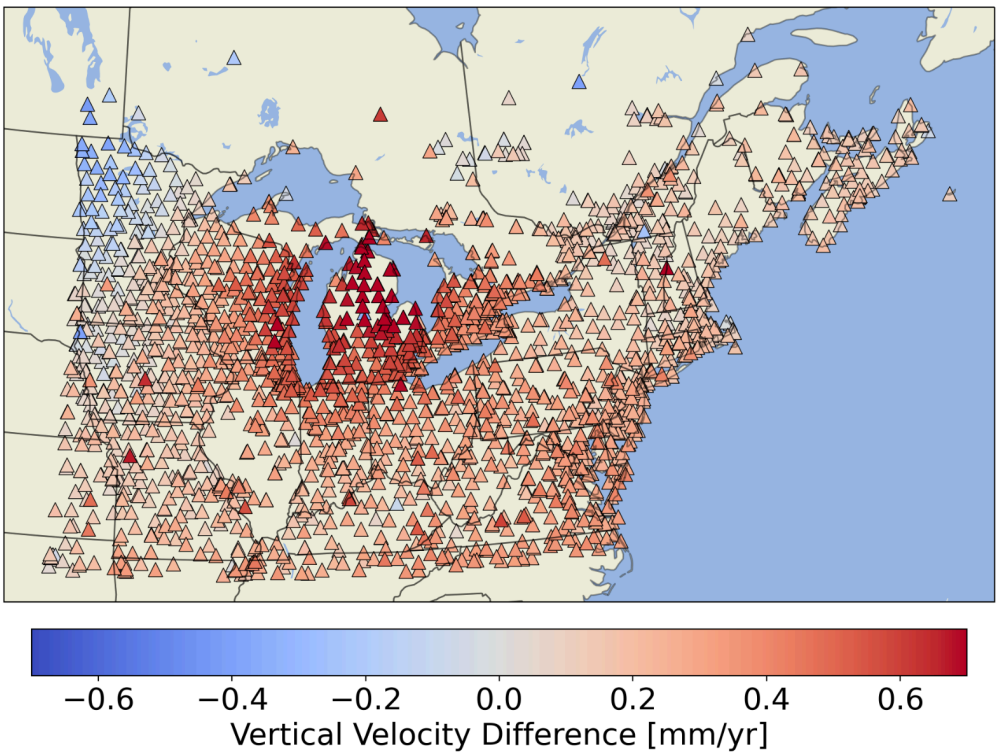

Figure 3.14: Vertical velocity differences between CMC filtered uncorrected time series and CMC filtered NTAOL+GRACE corrected time series.

3.5 Differences between GRACE and LAKE corrections

Variance reduction and velocity differences in NTAOL+GRACE corrected and NTAOL+LAKE corrected time series were compared in order to evaluate the effect of correcting for lake loading. Only time series that have been CMC filtered and that have a LAKE variance >1 mm in the vertical component are compared, in order to see if there is any additional benefit in using LAKE corrections instead of GRACE corrections for stations closest to the Great Lakes.

Figure 3.15 shows the variance reduction for the east component when applying LAKE instead of GRACE. There is noticeable reduction in variance in stations situated on the eastern and western shores of the Great Lakes. However, because the overall variance in filtered time series is small, the actual change in variance is also small. The north and vertical components of variance reductions are not shown because there is almost no change in variance for those components.

Figures 3.16, 3.17 and 3.18 show velocity differences between GRACE corrected and LAKE corrected time series for the east, north and vertical components, respectively. In the east components velocity differences are greater for stations closer to the Great Lakes, and the sign of the difference is dependent on if it is on the eastern or western shore. Velocity differences in the north component are negative for almost every station, but the magnitude varies depending on whether the station is on the northern or southern shore of the lakes. The overall negative velocity differences could be due to farther field loading effects captured in the GRACE corrections that are not represented when just considering lake loading, but more investigation is needed to determine the exact cause of this difference. Vertical velocity differences are greatest for stations right on the shores and on islands in the Great Lakes. The LAKE model is based on water levels within the Great Lakes and does not consider hydrological loading on land, and because of this the LAKE corrections probably do not accurately capture the vertical motions of stations farther

away from the lakes shores. This can be seen in Figure 3.18. where the sign of the velocity difference changes from positive to negative moving away from the lake shores. Histograms of the velocity differences for each component are shown in Figure 3.19. Differences are generally small, being within 0.1 mm/yr, 0.2 mm/yr and 0.25 mm/yr for the east, north, and vertical components, respectively.

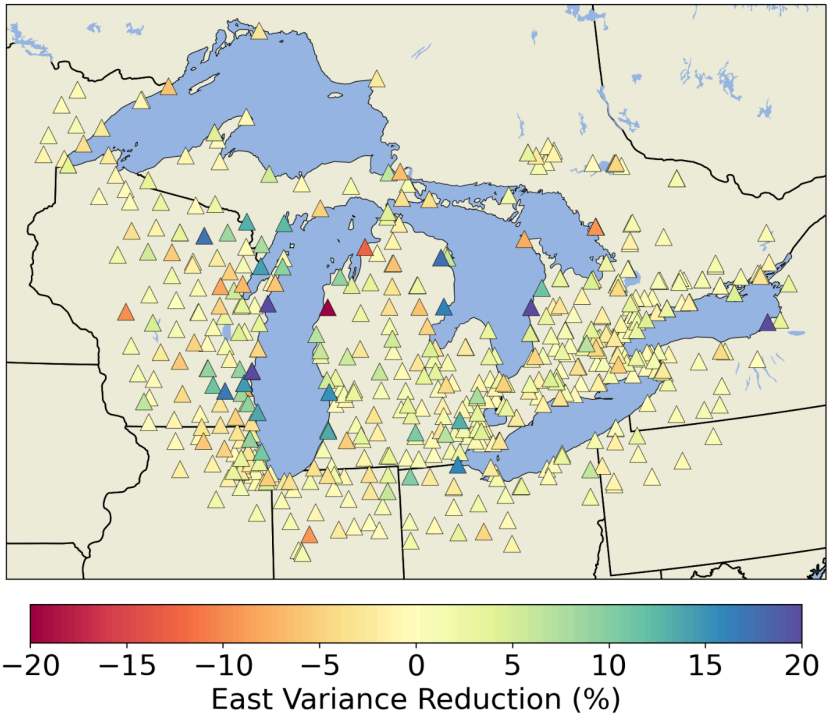

Figure 3.15: Variance reduction when using NTAOL+LAKE corrections versus NTAOL+GRACE corrections. All time series are CMC filtered.

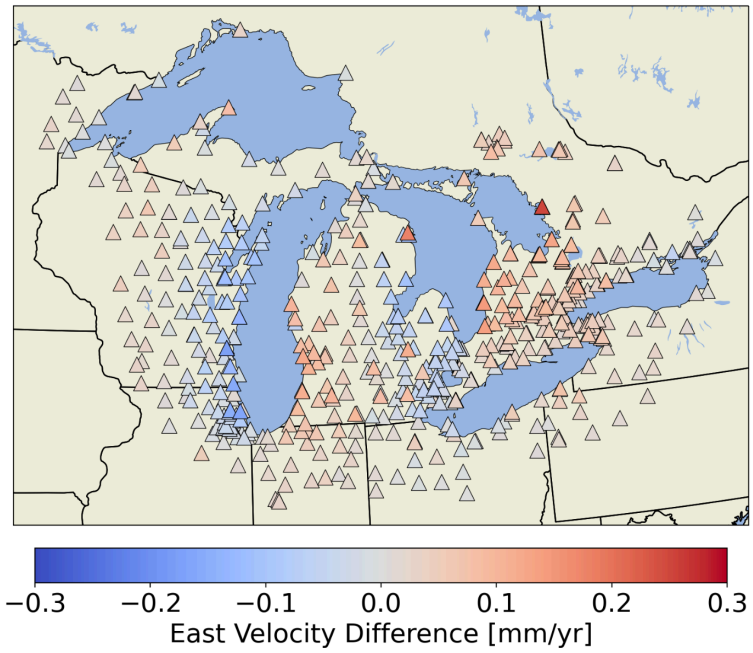

Figure 3.16: East component velocity differences when using LAKE instead of GRACE corrections. All time series are CMC filtered.

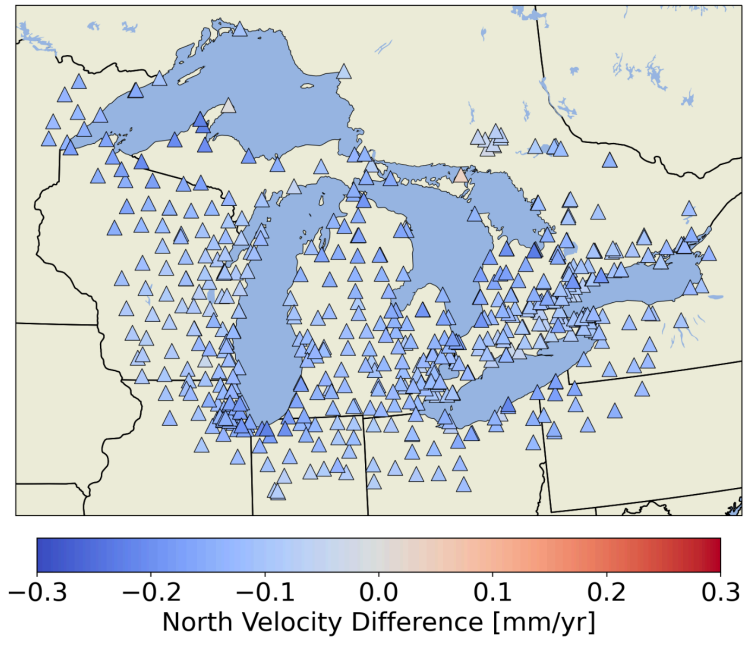

Figure 3.17: Same as Figure 3.16, but for the north component.

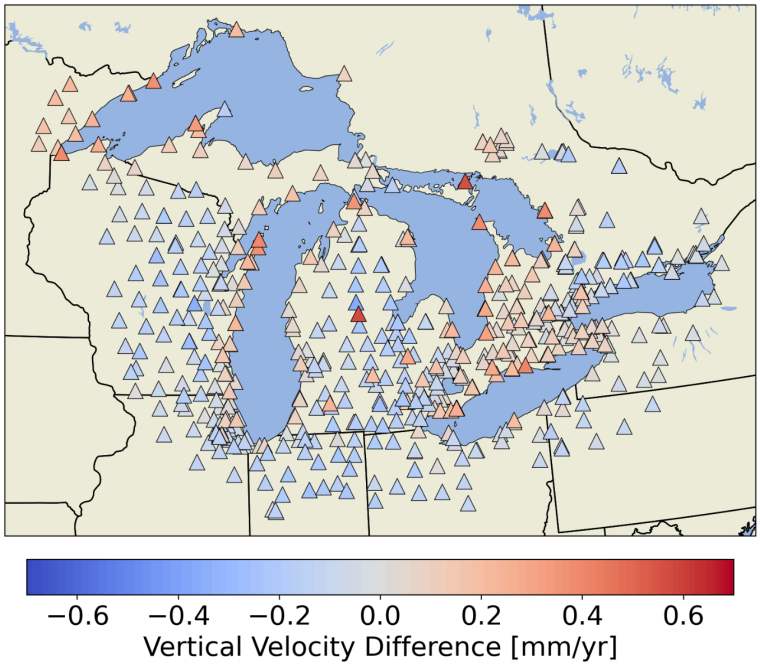

Figure 3.18: Same as Figure 3.16, but for the vertical component.

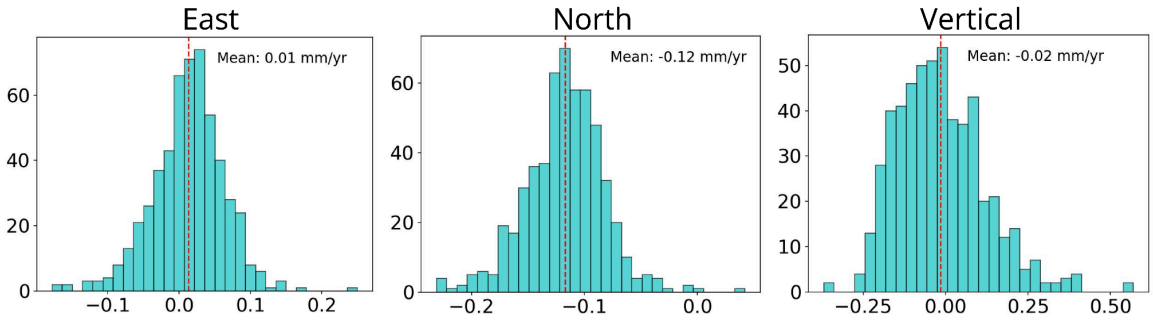

Figure 3.19: Histograms of the velocity differences when using LAKE instead of GRACE corrections.

3.6 Monument comparison

Monument information (see Section 2.3) for 831 stations in the study region is used to evaluate noise amplitudes and 8-year velocity uncertainties by monument type. Only the CMC

filtered and NTAOL+GRACE corrected time series are used, since stochastic variation due monument stability should not be spatially correlated with other GPS stations. Results are presented in Table 3.2. Most stations in the study region that have monument type information are either concrete pillar monuments or roof mounted monuments. The bedrock monument type particularly stands out when looking at RW amplitudes, with a median value of 0.0 mm/yr$^{1/2}$. However, FL amplitudes in bedrock monuments are much higher compared to other monument types and the median value for velocity uncertainty is 0.14 mm/yr, not significantly different from steel tower or roof mounted monuments. However, it is hard to make meaningful comparisons between bedrock monuments, DDBMs and steel tower monuments due to the limited sample size of those types. There is a clear difference between roof mounted monuments and concrete pillar monuments, with median velocity uncertainties of 0.15 mm/yr and 0.21 mm/yr, respectively. The concrete pillars have a significantly higher RW amplitude compared to roof mounted monuments, which suggests that concrete pillar monuments are less stable than monuments attached to roofs.

Table 3.2: Comparison of the noise amplitudes and velocity uncertainties of different monument types used by GPS stations in the study region.

type	# Stations	WN Amplitude [mm]	FL Amplitude [mm/yr^(1/4)]	RW Amplitude [mm/yr^(1/2)]	Uncertainty [mm/yr]
Bedrock	12	1.17	3.52	0.00	0.14
Concrete Pillar	314	1.27	1.62	0.57	0.21
DDBMs	11	1.28	1.79	0.57	0.21
Roof	461	1.45	1.84	0.38	0.15
Steel Tower	33	1.42	1.97	0.38	0.14

Concrete pillar monuments are mostly used in the state networks of Michigan, Wisconsin, Minnesota and Missouri, and each state network potentially uses a different design for the concrete pillar monuments. In order to see if there is a difference between concrete pillars used in different state networks, we compare the noise amplitudes and velocity uncertainties of only the concrete pillar monuments, but grouped by state. The results of this comparison are in Table 3.3. From these results there is a clear difference between concrete pillar monuments used in different states. Concrete pillar monuments in Michigan outperform all other concrete pillar monuments when looking at velocity uncertainty, with a median value of 0.1 mm/yr. This is less than the median values of velocity uncertainty for roof mounted monuments, and suggests that roof monuments are not inherently more stable than concrete pillar monuments, but that the design of the concrete pillar monument is an important factor for station stability. The concrete pillar monuments used in Wisconsin, Minnesota and Missouri have much higher velocity uncertainties compared to Michigan and other states, with median values of 0.28 mm/yr, 0.35 mm/yr and 0.28 mm/yr, respectively, which can be mainly attributed to the higher RW amplitudes in those monuments.

Table 3.3: Same as Table 3.2, but a comparison of only concrete pillar monuments grouped by different state networks.

type	# Stations	WN Amplitude [mm]	FL Amplitude [mm/yr^(1/4)]	RW Amplitude [mm/yr^(1/2)]	Uncertainty [mm/yr]
Michigan	88	1.14	1.14	0.19	0.10
Minnesota	34	1.19	2.14	0.96	0.35
Missouri	66	1.48	1.68	0.67	0.28
Other	65	1.50	1.79	0.19	0.13
Wisconsin	61	1.18	1.79	0.76	0.28

Minnesota uses an almost even mix of roof mounted monuments and concrete pillar monuments, which can be compared to one another to evaluate both types of monuments within a single state network. Results are presented in Table 3.4, which shows that roof mounted monuments have a velocity uncertainty more than 50% lower than the concrete pillar monuments in Minnesota. Given our comparison of concrete pillar monuments in different states, this is mostly likely due to the design of the concrete pillar monuments used in Minnesota.

Table 3.4: Same as Table 3.2, but only for monuments within Minnesota.

type	# Stations	WN Amplitude [mm]	FL Amplitude [mm/yr^(1/4)]	RW Amplitude [mm/yr^(1/2)]	Uncertainty [mm/yr]
Concrete Pillar	34	1.19	2.14	0.96	0.35
Roof	23	1.23	2.23	0.38	0.16

Chapter 4: Discussion

4.1 Masking of WN and RW amplitudes in GPS time series

This masking effect that NTAOL has on estimated WN amplitudes was first reported by Gobron et al. (2021) in their study of 10,000 globally distributed GPS stations. In this study, it is shown that this is also true for the estimated RW amplitudes. The masking of RW amplitudes is especially concerning, since the presence of RW has a bigger impact than WN and FL on the velocity uncertainties in long running stations. In addition to NTAOL masking RW amplitudes, the results also suggest that there is additional masking of RW due to other spatially correlated signals in the GPS time series, which can be seen in the results from CMC filtering (Figure 3.10). Filtering removes much of the FL present in the time series, and there is a slight increase in RW amplitudes after filtering, although not to the extent seen after removing NTAOL. A possible explanation for the masking effect is that for a given RW amplitude, a higher FL amplitude increases the time span of observations required to properly resolve that RW amplitude (Langbein and Svarc, 2019). So it could be that by removing FL with CMC filtering we decrease the

detection threshold for RW and therefore see more of the RW present in some time series. This means it is critical to remove mass loading and CMC filter the time series in order to properly resolve the RW amplitudes that may be due to monument instability. A potential improvement to this study would utilize the full time spans of the time series in order to properly resolve the noise characteristics.

A potential major limitation to this study is the use of only the WN+FL+RW stochastic model. If the stochastic behavior of a time series cannot be adequately described by this model, then the estimated stochastic parameters could potentially be biased, as was found in Gobron et al. (2021). However, time series that have been corrected for NTAOL fit the WN+PL model much better (Gobron et al., 2021), and that stochastic model is similar to the WN+FL+RW model used in this study. A more robust investigation would find the best fitting stochastic model for each time series, and then estimate velocity uncertainties from that model.

4.2 Horizontal displacements in the GRACE model

It was noticed that the GRACE horizontal corrections explained very little of the variance in the GPS time series, particularly around the Great Lakes. This is especially evident when comparing the GRACE horizontal corrections to the LAKE horizontal corrections, which explains significantly more of the variance in the time series immediately around the lakes (Figure 3.1). Figure 4.1 shows an example of this for the east component of station KEEE, which is on the western shore of Lake Michigan. In some cases the difference between GRACE and LAKE horizontal corrections can be >1 mm. Part of this discrepancy could be explained by the spatial resolution of the GRACE data, which is ~300km. The lower spatial resolution of GRACE could be spreading out the loading signal due to the Great Lakes, and this spreading out of the

loading gradient could diminish the effect of loading in the horizontal components. The difference is not seen to such an extent in the vertical component and variance differences between LAKE corrected and GRACE corrected time series are small for stations immediately next to the Great Lakes. The difference in the horizontal variance reduction implies that there may be more benefit in using loading models based on lake loading when correcting the horizontal components of stations next to large lakes, at least until hydrological loading models with higher spatial resolution are developed.

There are also horizontal velocity differences between LAKE corrected and GRACE corrected time series, even after CMC filtering (Figures 3.16, 3.17 and 3.18). This could be critical in the Great Lakes region when using GPS to calculate the strain field due to GIA (Kreemer et al., 2018). Not properly accounting for inter-annual variations in lake loading could potentially bias the GPS estimates of dilatational strain rates due to GIA.

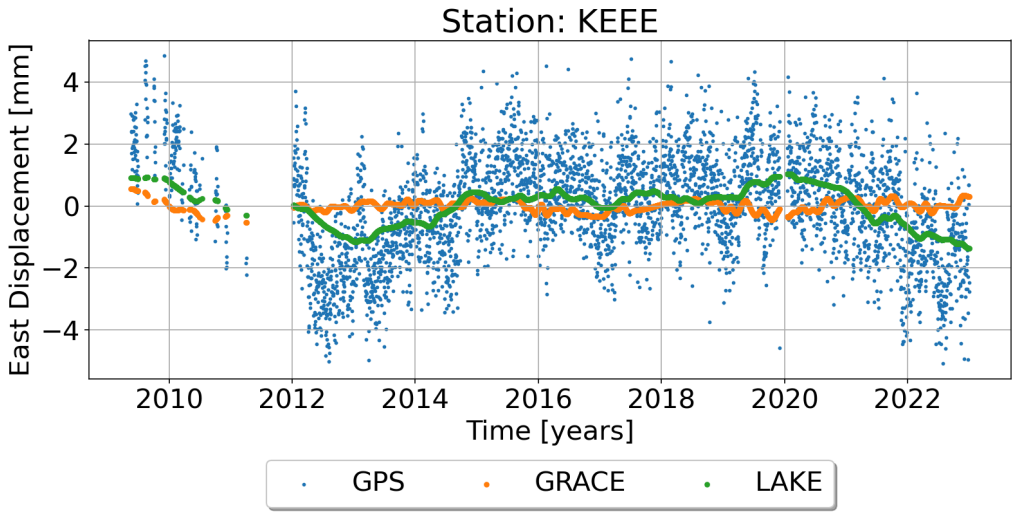

Figure 4.1: The east component of station KEEE plotted with the predicted GRACE and LAKE corrections.

4.3 CMC Filtering versus correcting for surface mass loading

Variance differences between uncorrected CMC filtered time series and loading corrected CMC filtered time series are very small (Figure 3.3), meaning that most of the variance due to mass loading is removed during the filtering process. Furthermore, there is the additional benefit of removing all spatially correlated noise, even noise due to processing errors and errors within the GPS infrastructure itself, during the CMC filtering process. However, long term hydrological loading rates still need to be corrected in CMC filtered time series, which can either be done by correcting the daily observations as was done in this study, or by estimating the long term trend in the surface mass loading models and using this value to correct the velocity estimate of the CMC filtered uncorrected time series. Future studies could compare the differences between quicker filtering methods and the more computationally intensive method, CMC Imaging, used in this study.

4.4 Potential limitations of the monument comparison

There are some potential limitations to the monument comparison presented in this thesis. The first limitation is due to the full time spans of the GPS time series not being used. If we used the full time spans, instead of limiting it to the time period of 2005 - 2023 used in this study, we could potentially resolve even smaller RW amplitudes, as mentioned in Section 4.1. However, the time span of almost 18 years used in this study should be sufficient for comparing large differences in RW amplitude. Using the full time period would also require much more computation time. The second limitation is due to the small sample size of monument types other than roof mounted and concrete pillar monuments. An improvement to this study would be to use

all stations available in the NGL database along with the station monument file to have a larger sample and more monument types for the comparison. Finally, as mentioned in Section 2.7, there is a chance that offsets were missed when visually inspecting the time series. Uncorrected offsets would influence the RW amplitudes of the time series, and could potentially bias the results of the monument comparison. However, the sample size of concrete pillar monuments and roof mounted monuments is probably large enough that the comparisons between those monument types is fairly robust. For better results, automatic offset detection algorithms (Gazeaux et al., 2013) will need to be improved so that large comparisons (i.e. using all of the NGL database) can be made without offsets influencing the results.

4.5. Seasonal signals in Wisconsin and Minnesota

During my analysis of the station time series around the Great Lakes, I performed a phase comparison between the vertical components of the GPS and GRACE signals (Figure 4.2). The results of the comparison revealed distinct differences between the networks of some states/provinces. This is most notable for stations in Wisconsin, Minnesota and the Ontario Peninsula, where the seasonality of GPS vertical displacements is ~90 days offset from the vertical displacement predicted by GRACE. The phase offset between GPS and GRACE in Wisconsin is mentioned in the results of Argus et al. (2020), but is not explored further. Also seen in my results is a phase offset of almost ~180 days along the Atlantic Coastal Plain, which is believed to be undergoing a porous response due to the withdrawal of groundwater in the region (Karegar et al., 2016).

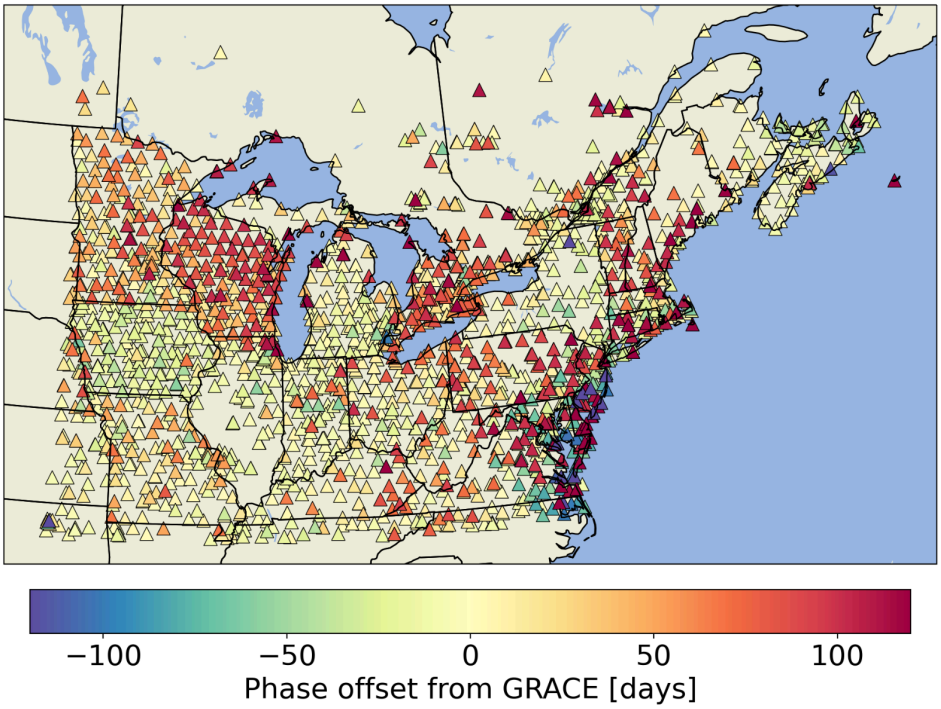

Figure 4.2: Vertical component phase offset from the GRACE predicted displacements

When looking at individual station time series, it was noticed that stations in Wisconsin, Minnesota, and the Ontario Peninsula had annual signals with peaks during the coldest period of the year in those regions. This led us to perform a correlation with temperature. To do this I used gridded mean temperature data from the NCEP-NCAR Reanalysis 1 dataset provided by NOAA PSL (Kalnay et al., 2018; https://psl.noaa.gov). Vertical displacement correlations with inverse temperature at the nearest grid point are shown in Figure 4.3. In general, the spatial pattern of correlation is consistent with the pattern of phase offset seen in Figure 4.2, with mostly positive correlations seen in Wisconsin and Minnesota. However, only a few stations located in the Ontario Peninsula show positive correlation. These results lead us to believe that temperature may be responsible for the annual seasonal signals in some stations. This is particularly noticeable for individual stations, an example of which is shown for PHPS in Figure 4.4, which is located in

northern Wisconsin. The station MIIR in Michigan is located only 34 kilometers from PHPS but does not show the same correlation with temperature. This temperature seasonal signal is also seen in the horizontal components of some stations, for example COTN in northern Minnesota (Figure 4.5).

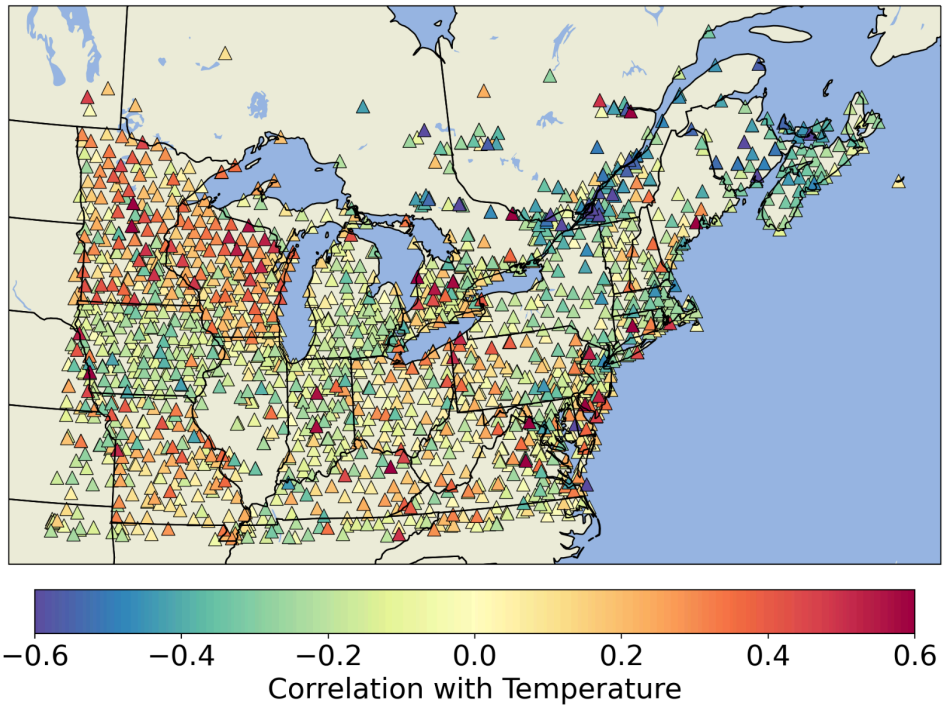

Figure 4.3: Vertical time series correlation with inverse temperature

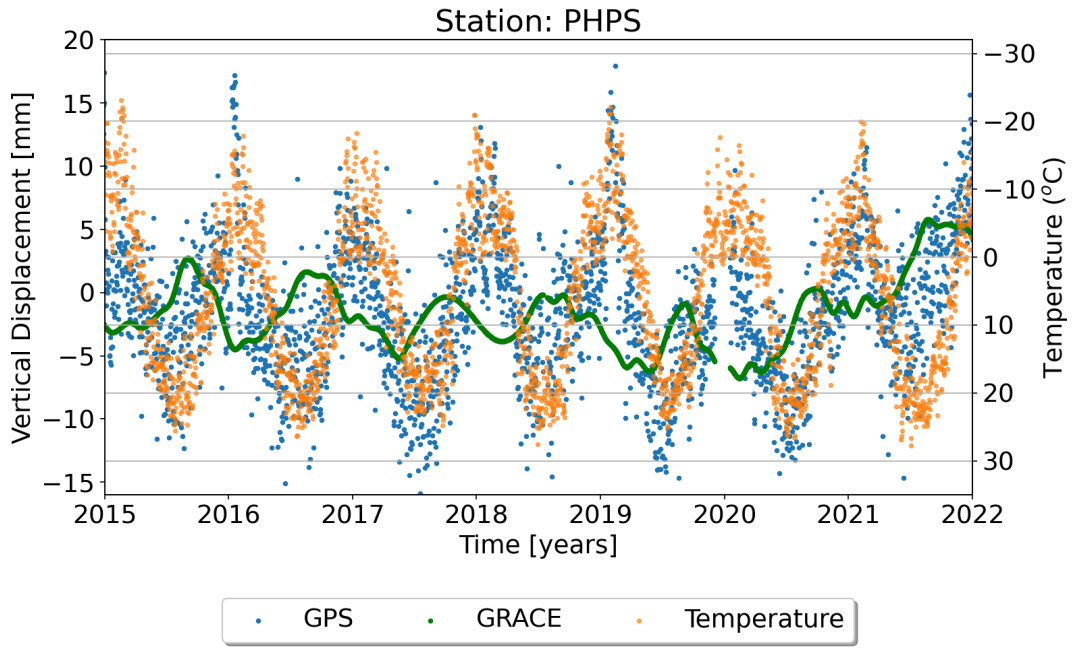

Figure 4.4: Vertical component of PHPS, located in northern Wisconsin. Note that temperature is inverse.

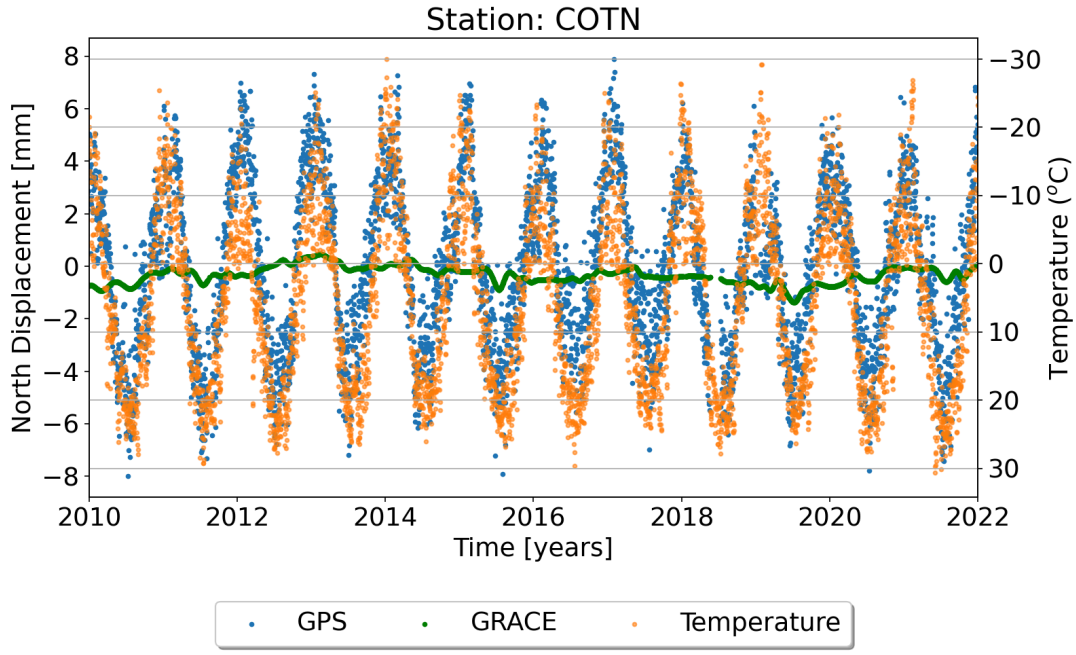

Figure 4.5: North component of COTN, located in northern Minnesota.

If a station's seasonal signal is controlled by temperature, then it can not be used to infer seasonal hydrologic loading. In an attempt to correct for this temperature seasonal signal, the phase from the temperature time series was estimated. The estimated phase of the temperature time series was then used to estimate the amplitude of an annual seasonal signal in the GPS time series (Figure 4.6). When this temperature seasonal signal is removed from the vertical time series, the corrected time series is much more consistent with hydrological loading from GRACE (Figure 4.7). The amplitude of the seasonal signal in phase with temperature is shown for all stations in Figure 4.8.

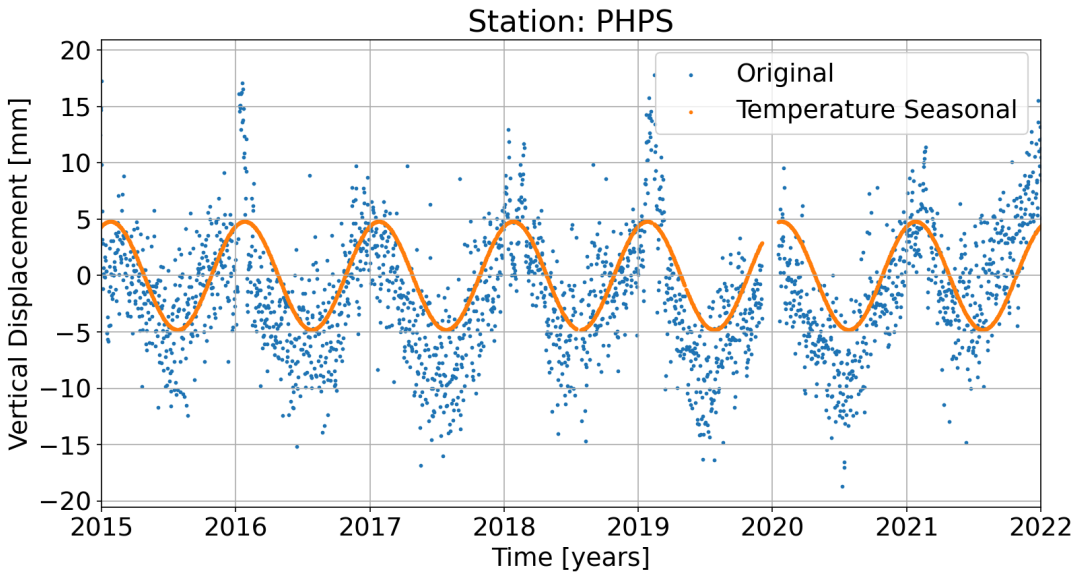

Figure 4.6: The vertical time series of PHPS with the estimated seasonal signal constrained to be in phase with temperature.

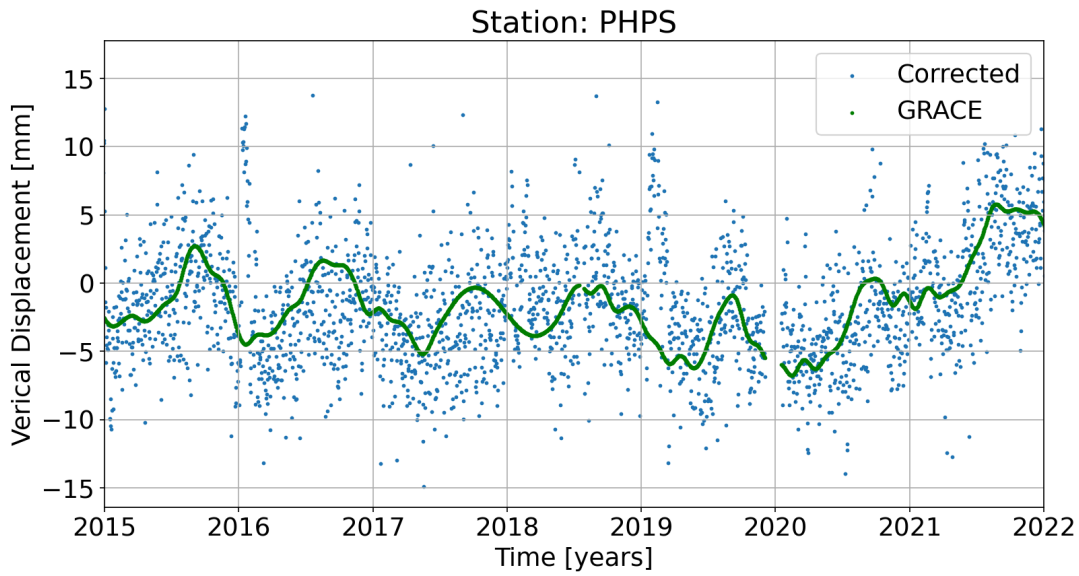

Figure 4.7: The vertical time series of PHPS with the estimated temperature seasonal signal removed, plotted with the predicted vertical displacements from GRACE.

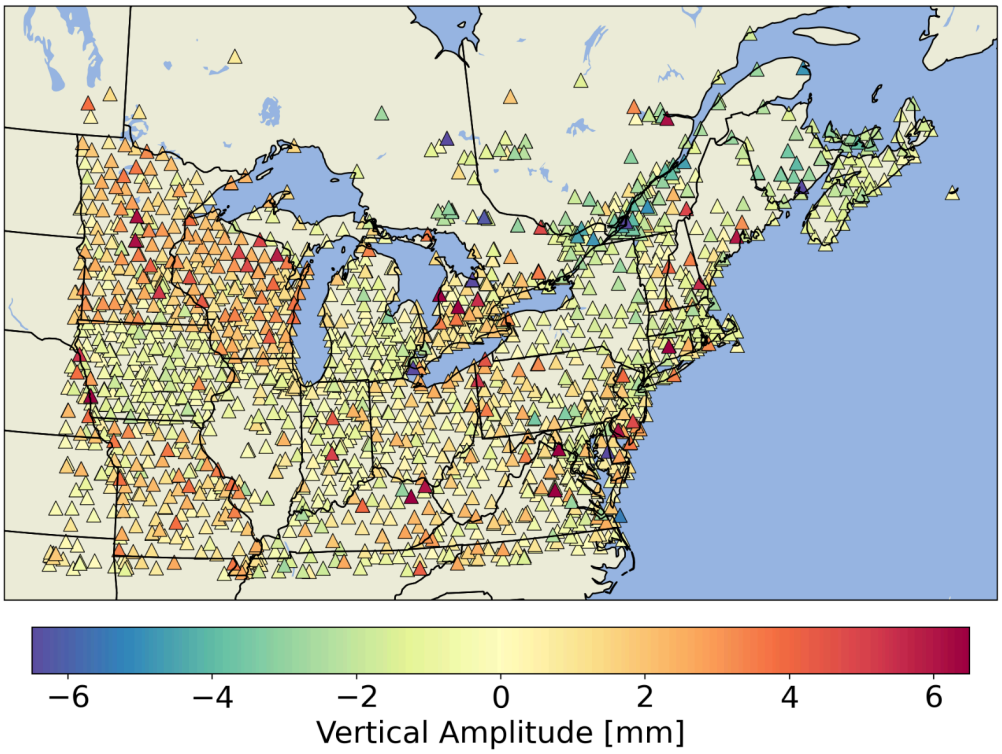

Figure 4.8: Vertical amplitude of the GPS annual seasonal signal in phase with temperature.

While the time series corrected with the temperature seasonal signal is much more consistent with the GRACE predicted displacements from hydrologic loading, it should be mentioned that this approach has the potential to remove any seasonal loading signals that are in phase with temperature. In order to evaluate the potential of this happening for stations in the study region, The phase offset between temperature and GRACE (Figure 4.9), and between temperature and LAKE (Figure 4.10) is calculated. While the phase offset between temperature and GRACE is always consistently ~100 days or more, the phase offset between temperature and LAKE is only a few days for some stations closest to the Great Lakes. This means there is potential to remove seasonality due to lake loading from stations immediately around the Great Lakes, and in order to preserve this lake loading seasonality a different approach is needed.

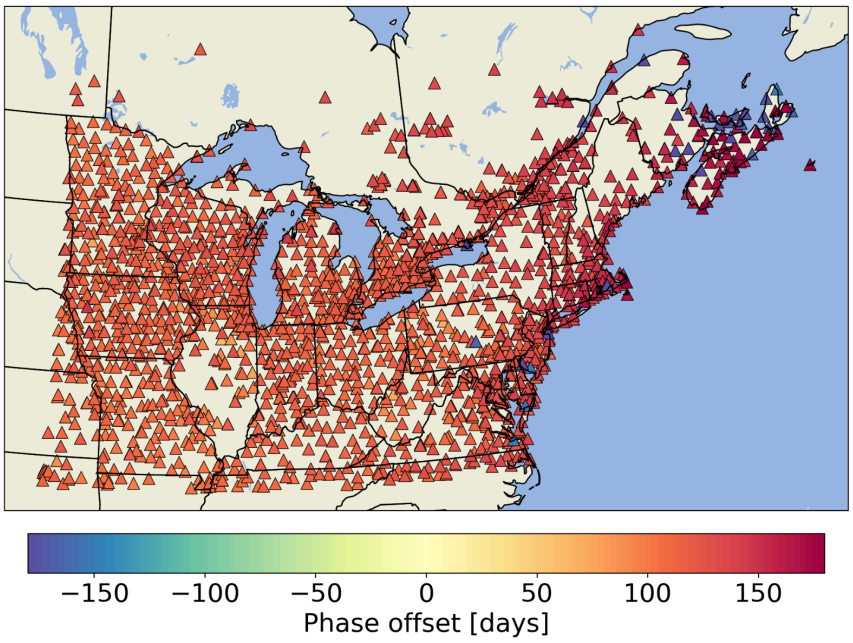

Figure 4.9: Phase offset between temperature and GRACE.

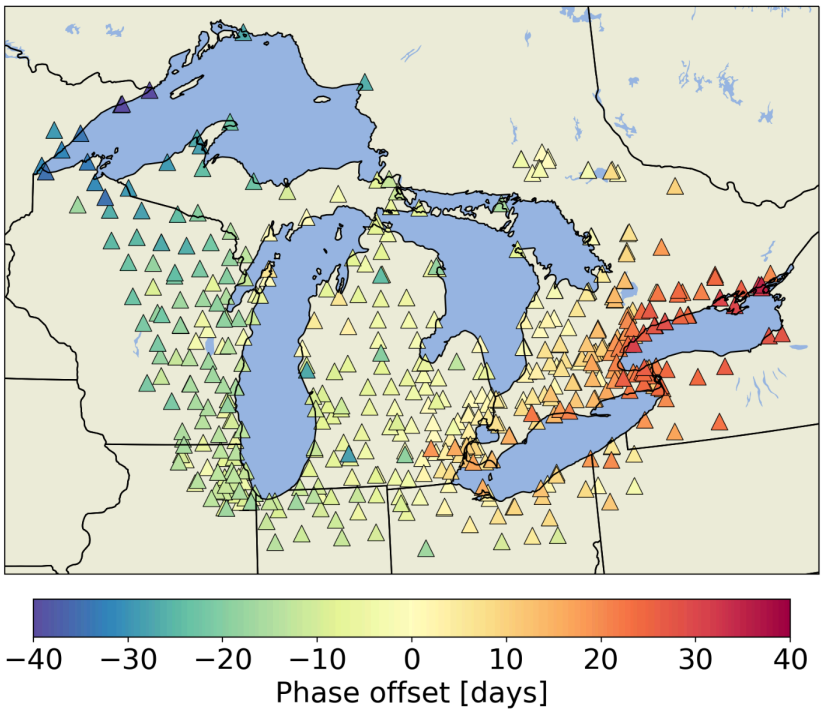

Figure 4.10: Phase offset between temperature and LAKE. Only stations that have a LAKE vertical variance of 1 mm or greater are shown.

The origin of the seasonal signal in phase with temperature is still not understood. It was speculated that it could be related to monument type since it is most consistently seen in stations with concrete pillar monuments. A comparison between monument types in Wisconsin and Minnesota only shows slight differences in the amplitude of the temperature seasonal signal (Figure 4.11), and obvious seasonal signals in phase with temperature in roof mounted stations was found on further inspection. Some explanations for temperature related seasonal signals have been made in previous studies, such as snow intrusion within the GPS antenna (Koulali and Clarke, 2020) or elevation changes due to freeze/thaw of the ground (Liu and Larson, 2018), but more work is needed to identify the cause of this signal and why it seems to only affect some state networks.

These results underscore the potential danger in overinterpreting seasonal signals in GPS time series, a warning echoed by others (Chanard et al., 2020). More work is needed in identifying the origin of and correcting for anomalous seasonal signals in GPS time series, so that more stations can be used to study seasonal patterns in hydrological loading.

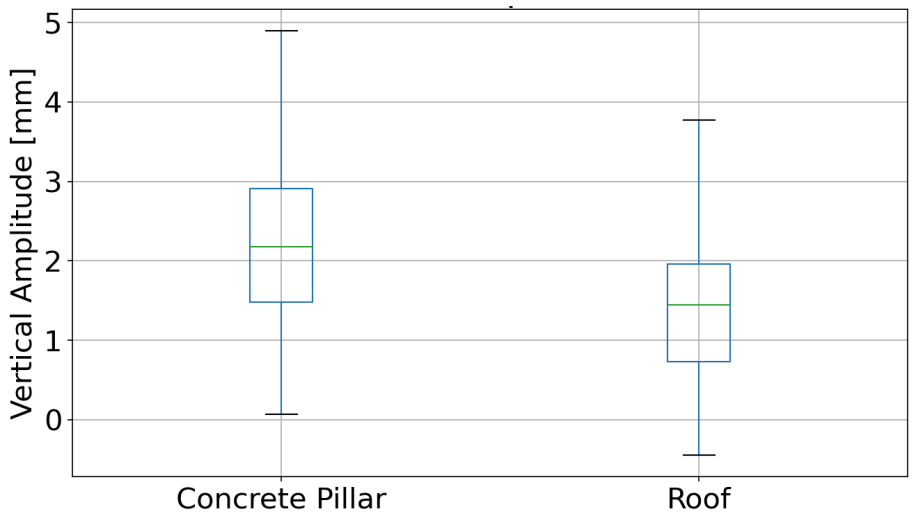

Figure 4.11: Comparison of the vertical amplitude of the temperature seasonal signal in concrete pillar (n = 88) and roof (n = 38) monuments in Wisconsin and Minnesota.

Chapter 5: Conclusion

In this thesis it is shown that correcting GPS time series for surface mass loading is critical to estimating station velocities with realistic uncertainties. Failure to correct for surface mass loading not only results in higher overall velocity uncertainties, but also an underestimation of velocity uncertainties in stations with significant RW. Furthermore, it was shown that CMC filtering is sufficient at removing variance due to surface mass loading, as well as additional spatially correlated noise, which lowers FL amplitudes and reveals more RW amplitude in some GPS time series. However, the long term trends from surface mass loading, especially hydrological loading, needs to be corrected when using GPS time series for studying geophysical processes, such as GIA, even in CMC filtered time series. Some additional improvement can be gained by using models of loading due to water mass variations within the Great Lakes, but only for stations closest to the lake shores. Finally, a comparison of monument types shows that roof mounted monuments perform better than concrete pillar monuments, but that the design of the concrete pillar monuments highly influences their stability. Concrete pillar monuments in

Michigan perform better than most roof mounted monuments, while those in Wisconsin, Minnesota and Missouri perform significantly worse, when comparing velocity uncertainties.

Results from this study may also be useful for determining the suitability of GPS stations for use in scientific research or surveying applications. Estimated noise amplitudes are another metric that could be used to flag and remove outlier stations, but care should be taken for this approach. If using GPS to study a signal that has properties that are like RW, such as hydrological loading, then using RW amplitudes to filter stations could remove stations that have the signal of interest. However, for studying long term geophysical motions it may be useful to remove such stations.

From the CMC filtering results it is apparent that surface mass loading does not account for all of the spatially correlated noise in GPS time series. This research can be expanded on in the future by investigating the differences between surface mass loading corrected time series and CMC filtered time series, in order to understand the portion of the spatially correlated noise not accounted for by the surface mass loading models. Gobron et al. (2024), looking at the spatiotemporal correlations of noise in the surface mass loading corrected NGL GPS daily time series, determined that a significant portion of both WN and FL is correlated at large scales (>150km) and correlations do not reach 0.0 at even the largest distances. This suggests noise sources related to the processing of the GPS observations, and looking at how the processing strategy affects noise characteristics in the daily time series is a potential next step for continuing this research.

References

Amiri-Simkooei, A. R. (2009). Noise in multivariate GPS position time-series. Journal of Geodesy, 83, 175-187.

Amiri-Simkooei, A. R. (2016). Non-negative least-squares variance component estimation with application to GPS time series. Journal of Geodesy, 90, 451-466.

Amiri-Simkooei, A. R., Mohammadloo, T. H., & Argus, D. F. (2017). Multivariate analysis of GPS position time series of JPL second reprocessing campaign. Journal of Geodesy, 91, 685-704.

Argus, D. F., Landerer, F. W., Wiese, D. N., Martens, H. R., Fu, Y., Famiglietti, J. S., ... & Watkins, M. M. (2017). Sustained water loss in California's mountain ranges during severe drought from 2012 to 2015 inferred from GPS. Journal of Geophysical Research: Solid Earth, 122(12), 10-559.

Argus, D. F., Ratliff, B., DeMets, C., Borsa, A. A., Wiese, D. N., Blewitt, G., ... & Landerer, F. W. (2020). Rise of Great Lakes surface water, sinking of the upper Midwest of the United States, and viscous collapse of the forebulge of the former Laurentide ice sheet. Journal of Geophysical Research: Solid Earth, 125(9), e2020JB019739.

Argus, D. F., Martens, H. R., Borsa, A. A., Knappe, E., Wiese, D. N., Alam, S., ... & Gardiner, W. P. (2022). Subsurface water flux in California's Central Valley and its source watershed from space geodesy. Geophysical Research Letters, 49(22), e2022GL099583.

Blewitt, G., & Lavallée, D. (2002). Effect of annual signals on geodetic velocity. Journal of Geophysical Research: Solid Earth, 107(B7), ETG-9.

Blewitt, G., W. C. Hammond, and C. Kreemer (2018), Harnessing the GPS data explosion for interdisciplinary science, Eos, 99, https://doi.org/10.1029/2018EO104623.

Bock, Y., & Melgar, D. (2016). Physical applications of GPS geodesy: A review. Reports on Progress in Physics, 79(10), 106801.

Borsa, A. A., Agnew, D. C., & Cayan, D. R. (2014). Ongoing drought-induced uplift in the western United States. Science, 345(6204), 1587-1590.

Chanard, K., Métois, M., Rebischung, P., & Avouac, J. P. (2020). A warning against over-interpretation of seasonal signals measured by the Global Navigation Satellite System. Nature Communications, 11(1), 1375.

Dill, R., Dobslaw, H. (2018): ESMGFZ: Operational Model Products for Geodetic Applications, (Geophysical Research Abstracts ; Vol. 20, EGU2018-2772, 2018), General Assembly European Geosciences Union (Vienna 2018).

Dong, D., Fang, P., Bock, Y., Webb, F., Prawirodirdjo, L., Kedar, S., & Jamason, P. (2006). Spatiotemporal filtering using principal component analysis and Karhunen‐Loeve expansion approaches for regional GPS network analysis. Journal of geophysical research: solid earth, 111(B3).

Dyke, A. S., & Prest, V. K. (1987). Late Wisconsinan and Holocene history of the Laurentide ice sheet. Géographie physique et Quaternaire, 41(2), 237-263.

Gazeaux, J., Williams, S., King, M., Bos, M., Dach, R., Deo, M., ... & Webb, F. H. (2013). Detecting offsets in GPS time series: First results from the detection of offsets in GPS experiment. Journal of Geophysical Research: Solid Earth, 118(5), 2397-2407.

Gobron, K., Rebischung, P., Van Camp, M., Demoulin, A., & de Viron, O. (2021). Influence of aperiodic non‐tidal atmospheric and oceanic loading deformations on the stochastic properties of global GNSS vertical land motion time series. Journal of Geophysical Research: Solid Earth, 126(9), e2021JB022370.

Gobron, K., Rebischung, P., Chanard, K., & Altamimi, Z. (2024). Anatomy of the spatiotemporally correlated noise in GNSS station position time series. Journal of Geodesy, 98(5), 34.

Hammond, W. C., Blewitt, G., Kreemer, C., & Nerem, R. S. (2021). GPS imaging of global vertical land motion for studies of sea level rise. Journal of Geophysical Research: Solid Earth, 126(7), e2021JB022355.

He, X., Montillet, J. P., Fernandes, R., Bos, M., Yu, K., Hua, X., & Jiang, W. (2017). Review of current GPS methodologies for producing accurate time series and their error sources. Journal of Geodynamics, 106, 12-29.

He, X., Montillet, J. P., Hua, X., Yu, K., Jiang, W., & Zhou, F. (2017). Noise analysis for environmental loading effect on GPS position time series. Acta geodynamica et geomaterialia, 14(1), 131-142.

He, X., Bos, M. S., Montillet, J. P., & Fernandes, R. M. S. (2019). Investigation of the noise properties at low frequencies in long GNSS time series. Journal of Geodesy, 93(9), 1271-1282.

He, X., Bos, M. S., Montillet, J. P., Fernandes, R., Melbourne, T., Jiang, W., & Li, W. (2021). Spatial variations of stochastic noise properties in GPS time series. Remote Sensing, 13(22), 4534.

Johnson, H. O., & Agnew, D. C. (1995). Monument motion and measurements of crustal velocities. Geophysical Research Letters, 22(21), 2905-2908.

Kalnay, E., Kanamitsu, M., Kistler, R., Collins, W., Deaven, D., Gandin, L., ... & Joseph, D. (2018). The NCEP/NCAR 40-year reanalysis project. In Renewable energy (pp. Vol1_146-Vol1_194). Routledge.

Karegar, M. A., Dixon, T. H., & Engelhart, S. E. (2016). Subsidence along the Atlantic Coast of North America: Insights from GPS and late Holocene relative sea level data. Geophysical Research Letters, 43(7), 3126-3133.

Klos, A., Dobslaw, H., Dill, R., & Bogusz, J. (2021). Identifying the sensitivity of GPS to non-tidal loadings at various time resolutions: examining vertical displacements from continental Eurasia. GPS Solutions, 25(3), 89.

Koulali, A., & Clarke, P. J. (2020). Effect of antenna snow intrusion on vertical GPS position time series in Antarctica. Journal of Geodesy, 94(10), 101.

Kreemer, C., Hammond, W. C., & Blewitt, G. (2018). A robust estimation of the 3‐D intraplate deformation of the North American plate from GPS. Journal of Geophysical Research: Solid Earth, 123(5), 4388-4412.

Kreemer, C., Blewitt, G., & Davis, P. M. (2020). Geodetic evidence for a buoyant mantle plume beneath the Eifel volcanic area, NW Europe. Geophysical Journal International, 222(2), 1316-1332.

Kreemer, C., & Blewitt, G. (2021). Robust estimation of spatially varying common-mode components in GPS time-series. Journal of geodesy, 95(1), 13.

Langbein, J. (2008). Noise in GPS displacement measurements from Southern California and Southern Nevada. Journal of Geophysical Research: Solid Earth, 113(B5).

Langbein, J. (2012). Estimating rate uncertainty with maximum likelihood: differences between power-law and flicker–random-walk models. Journal of Geodesy, 86(9), 775-783.

Langbein, J., & Svarc, J. L. (2019). Evaluation of temporally correlated noise in Global Navigation Satellite System time series: Geodetic monument performance. Journal of Geophysical Research: Solid Earth, 124, 925–942. https://doi.org/10.1029/2018JB016783

Li, Z., Yue, J., Hu, J., Xiang, Y., Chen, J., & Bian, Y. (2018). Effect of surface mass loading on geodetic GPS observations. Applied Sciences, 8(10), 1851.

Liu, L., & Larson, K. M. (2018). Decadal changes of surface elevation over permafrost area estimated using reflected GPS signals. The Cryosphere, 12(2), 477-489.

Lomb, N. R. (1976). Least-squares frequency analysis of unequally spaced data. Astrophysics and space science, 39, 447-462.

Masson, C., Mazzotti, S., Vernant, P., & Doerflinger, E. (2019). Extracting small deformation beyond individual station precision from dense Global Navigation Satellite System (GNSS) networks in France and western Europe. Solid Earth, 10(6), 1905-1920.

Nikolaidis, R. (2002). Observation of geodetic and seismic deformation with the Global Positioning System. University of California, San Diego.

Norton, P. A., Driscoll, D. G., & Carter, J. M. (2019). Climate, streamflow, and lake-level trends in the Great Lakes Basin of the United States and Canada, water years 1960–2015 (No. 2019-5003). US Geological Survey.

Peltier, W. R. (1999). Global sea level rise and glacial isostatic adjustment. Global and planetary change, 20(2-3), 93-123.

Peltier, W. R., Argus, D. F., & Drummond, R. (2015). Space geodesy constrains ice age terminal deglaciation: The global ICE‐6G_C (VM5a) model. Journal of Geophysical Research: Solid Earth, 120(1), 450-487.

Ray, R. D., & Ponte, R. M. (2003). Barometric tides from ECMWF operational analyses. In Annales Geophysicae (Vol. 21, No. 8, pp. 1897-1910). Göttingen, Germany: Copernicus Publications.

Ray, J., Altamimi, Z., Collilieux, X., & van Dam, T. (2008). Anomalous harmonics in the spectra of GPS position estimates. GPS solutions, 12, 55-64.

Santamaría-Gómez, A., & Mémin, A. (2015). Geodetic secular velocity errors due to interannual surface loading deformation. Geophysical Journal International, 202(2), 763-767.

Save, H., Bettadpur, S., & Tapley, B. D. (2016). High‐resolution CSR GRACE RL05 mascons. Journal of Geophysical Research: Solid Earth, 121(10), 7547-7569.

Scargle, J. D. (1982). Studies in astronomical time series analysis. II-Statistical aspects of spectral analysis of unevenly spaced data. Astrophysical Journal, Part 1, vol. 263, Dec. 15, 1982, p. 835-853., 263, 835-853.

Tapley, B. D., Bettadpur, S., Ries, J. C., Thompson, P. F., & Watkins, M. M. (2004). GRACE measurements of mass variability in the Earth system. science, 305(5683), 503-505.

Tian, Y., & Shen, Z. K. (2016). Extracting the regional common‐mode component of GPS station position time series from dense continuous network. Journal of Geophysical Research: Solid Earth, 121(2), 1080-1096.

U.S. Environmental Protection Agency & Government of Canada. (1995). The Great Lakes. An Environmental Atlas and Resource Book (3rd Edition).

van Dam, T. M., & Herring, T. A. (1994). Detection of atmospheric pressure loading using very long baseline interferometry measurements. Journal of Geophysical Research: Solid Earth, 99(B3), 4505-4517.

van Dam, T. M., Blewitt, G., & Heflin, M. B. (1994). Atmospheric pressure loading effects on Global Positioning System coordinate determinations. Journal of Geophysical Research: Solid Earth, 99(B12), 23939-23950.

van Dam, T. M., & Wahr, J. (1998). Modeling environment loading effects: A review. Physics and Chemistry of the Earth, 23(9-10), 1077-1087.

van Dam, T., Collilieux, X., Wuite, J., Altamimi, Z., & Ray, J. (2012). Nontidal ocean loading: amplitudes and potential effects in GPS height time series. Journal of Geodesy, 86, 1043-1057.

Wang, L., Bevis, M., Peng, Z., Kaban, M. K., Thomas, M., & Chen, C. (2022). Tracking the source direction of surface mass loads using vertical and horizontal displacements from satellite geodesy: A case study of the inter-annual fluctuations in the water level in the Great Lakes. Remote Sensing of Environment, 274, 113001.

Wdowinski, S., Bock, Y., Zhang, J., Fang, P., & Genrich, J. (1997). Southern California permanent GPS geodetic array: Spatial filtering of daily positions for estimating coseismic and postseismic displacements induced by the 1992 Landers earthquake. Journal of Geophysical Research: Solid Earth, 102(B8), 18057-18070.

White, A. M., Gardner, W. P., Borsa, A. A., Argus, D. F., & Martens, H. R. (2022). A review of GNSS/GPS in hydrogeodesy: Hydrologic loading applications and their implications for water resource research. Water Resources Research, 58(7), e2022WR032078.

Williams, S. D. P. (2003). The effect of coloured noise on the uncertainties of rates estimated from geodetic time series. Journal of Geodesy, 76, 483-494.

Williams, S. D., Bock, Y., Fang, P., Jamason, P., Nikolaidis, R. M., Prawirodirdjo, L., ... & Johnson, D. J. (2004). Error analysis of continuous GPS position time series. Journal of Geophysical Research: Solid Earth, 109(B3).

Williams, S. D. P., & Penna, N. T. (2011). Non‐tidal ocean loading effects on geodetic GPS heights. Geophysical Research Letters, 38(9).

Wu, P., & Peltier, W. R. (1983). Glacial isostatic adjustment and the free air gravity anomaly as a constraint on deep mantle viscosity. Geophysical Journal International, 74(2), 377-449.

Wyatt, F. (1982). Displacement of surface monuments: horizontal motion. Journal of Geophysical Research: Solid Earth, 87(B2), 979-989.

Wyatt, F. K. (1989). Displacement of surface monuments: Vertical motion. Journal of Geophysical Research: Solid Earth, 94(B2), 1655-1664.

Xue, L., Fu, Y., & Martens, H. R. (2021). Seasonal hydrological loading in the Great Lakes region detected by GNSS: A comparison with hydrological models. Geophysical Journal International, 226(2), 1174-1186.

Zhang, L., Zhao, Y., Hein-Griggs, D., Barr, L., & Ciborowski, J. J. (2019). Projected extreme temperature and precipitation of the Laurentian Great Lakes Basin. Global and planetary change, 172, 325-335.